SYNTHESIS AND CHARACTERISATION OF NEW CYCLIC AND ACYCLIC FERROCENE PEPTIDE CONJUGATES

A Thesis Submitted to the College of

Graduate Studies and Research

In Partial Fulfillment of the Requirements

For the Degree of Master of Science

In the Department of Chemistry

University of Saskatchewan

Saskatoon

By

Mark Andrew Milne

Permission to Use

In presenting this thesis in partial fulfilment of the requirements for a Postgraduate degree from the University of Saskatchewan, I agree that the Libraries of this University may make it freely available for inspection. I further agree that permission for copying of this thesis in any manner, in whole or in part, for scholarly purposes may be granted by the professor or professors who supervised my thesis work or, in their absence, by the Head of the Department or the Dean of the College in which my thesis work was done. It is understood that any copying or publication or use of this thesis or parts thereof for financial gain shall not be allowed without my written permission. It is also understood that due recognition shall be given to me and to the University of Saskatchewan in any scholarly use which may be made of any material in my thesis.

Requests for permission to copy or to make other use of material in this thesis in whole or part should be addressed to:

Head of the Department of Chemistry

University of Saskatchewan

Saskatoon, Saskatchewan

S7N 5C9

ABSTRACT

In this thesis a series of diphenol phenanthroline (Dpp) peptide conjugates were synthesized and then coupled to ferrocene to give the corresponding organometallic conjugates. The first step of the synthesis was achieved by esterification of peptides with the phenol group of the Dpp. The next step was the removal of the protecting Boc group and the addition of ferrocene acid chloride at high dilutions to give the desired macrocycles of the type Dpp-$(peptide)_2$ Fc. (peptide = Leu-Leu (**3**), Leu-Leu-Leu (**5**)). However, the syntheses proceeded in low yields where only small quantities of the desired products were obtained. A suitable crystal of compound **3** was grown from $CHCl_3$ which shows a number of intra and intermolecular hydrogen bonding interactions between peptides strands.In addition, the system $[Dpp\text{-}Fc]_2$ (**1**) was syntheised by refluxing Dpp and $Fc[COCl]_2$ in dichloromethane. A suitable crystal was grown which has π-π interactions between intramolecular Dpp units as well as a number of CH-π interactions which determine the crystal packing. The electrochemical experiments on compound **1** show a cathodic shift upon addition of Zn^{2+} to a solution of **1**. This observation is believed to occur because of a conformational change in **1**.

The last area of synthesis that was done was the attempt at β-sheet formation using Fc as a scaffold to align peptide strands. Two systems were studied in this thesis [Fc(n'-AA-OMe)(1-AA)]$_2$-1,4butyl diamine. (AA =Ala (**8**), Gly (**9**)). Both were studied by ^{1}H NMR to evaluate the presence of hydrogen bonding interactions. The results indicate the presence of intramolecular H-bonding, which is believed to form β-sheet like structures in solution.

ACKNOWLEDGMENTS

I would like to thank my supervisor Dr. H.-B. Kraatz for his support and guidance during my years of study. I would also like to thank Dr. Foley for being on my advisory committee and the suggestions and support he gave me. I would like to acknowledge the help from Dr. Gabrielle Schatte and Dr. Michael Jennings for their help in solving crystal structures. Dr. Nadiene Merkley for her NMR help. Ken Thomas (U Saskatchewan) and Doug Hairsine (UWO) for their help with mass spectrometry, as well as all group members who gave their help and support.

DEDICATION

I would like to thank my family and friends who always believed in me.

TABLE OF CONTENTS

Page

LIST OF FIGURES

Page

LIST OF SCHEMES

Page

LIST OF TABLES

LIST OF ABBREVIATIONS

AA	amino acid
Å	angstrom
Ala	alanine
CD	circular dichroism
CV	cyclic voltammetry
DCC	dicyclohexylcarbodiimide
DCM	dichloromethane
DMAP	4-dimethylaminopyridine
Dpp	diphenol phenanthroline
EDC	1-ethyl-3-(3-dimethylaminopropyl)-carbodiimide
Fc	ferrocene
FCA	ferrocene amino acid
$Fc[COOH]_2$	ferrocene dicarboxylic acid
HBTU	O-benzotriazole-N,N,N’,N’-tetramethyl-uronium-hexafluoro-phosphate
HOBt	hydroxybenzotriazole
Gly	glycine
Leu	leucine
MS	mass spectrometry
TEA	triethyl amine
TFA	trifluoroacetic acid

CHAPTER 1.

INTRODUCTION

1.1 PEPTIDES

The dictionary defines a peptide as "two or more amino acids by combination of the amino group of one acid with the carboxyl group of another".[1] In this definition the term amino acid (AA) is used as component of a larger molecule. α-Amino acids are natural products that are comprised of an amino group and a carboxyl acid group both bound to a common carbon atom and a side chain usually denoted by R. This side chain alters the physical properties of the amino acid, such as its solubility, and influences the spatial orientation of a growing peptide chain. Figure 1.1 shows a few amino acids.

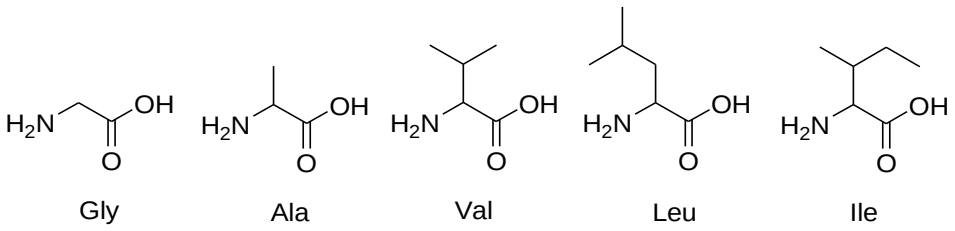

Figure 1.1. Drawing of glycine (Gly), alanine (Ala), valine (Val), leucine (Leu), and isoleucine (Ile).

All naturally occurring α-amino acids, except for glycine (Gly), have a stereogenic αC which creates the possibility of stereoisomers. The two isomers are denoted as L and D and, using Ala as an example, are shown in Figure 1.2. The L-isomer is common in Nature, while the D amino acids are less common.[2]

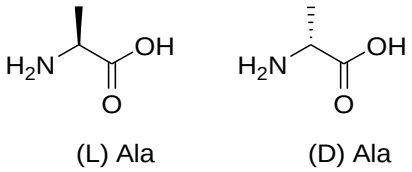

Figure 1.2. Drawing of L-Alanine and D-Alanine. When stereochemistry is not explicitly shown it is assumed that the amino acid drawn is an L-AA.

As amino acids are coupled together, either by enzymatic reactions or synthetic coupling reactions, amide bonds or peptide bonds are formed between the amide of one amino acid and the carboxyl group of the second amino acid (Figure 1.3). Coupling reagents can be described as activating compounds used in the synthesis of peptide bonds and a number of common agents will be discussed later in this thesis.

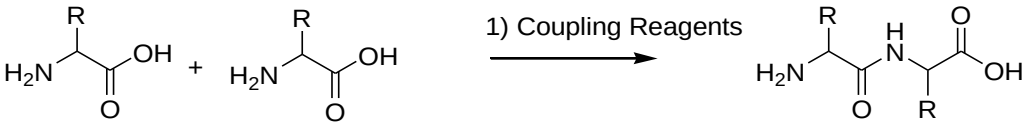

Figure 1.3. Reaction of two amino acids with side chains denoted by R using coupling reagents to form a peptide bond between the acid group of one amino acid and the amine group of the other amino acid.

As amino acids are coupled, they form a linear peptide strand. This peptide strand can then arrange into various secondary structures, stabilized by intramolecular hydrogen bonding interactions and the steric demand of the amino acid side chains. Hydrogen

bonding in peptide strands is the leading factor in folding of peptides and dictates the overall secondary structure. Common secondary structural elements found in proteins, including a β-sheet, an α-helix and various turns are shown in Figure 1.4. As secondary structures interact, a preferred structure is formed, which in turn determines the overall properties or the protein.

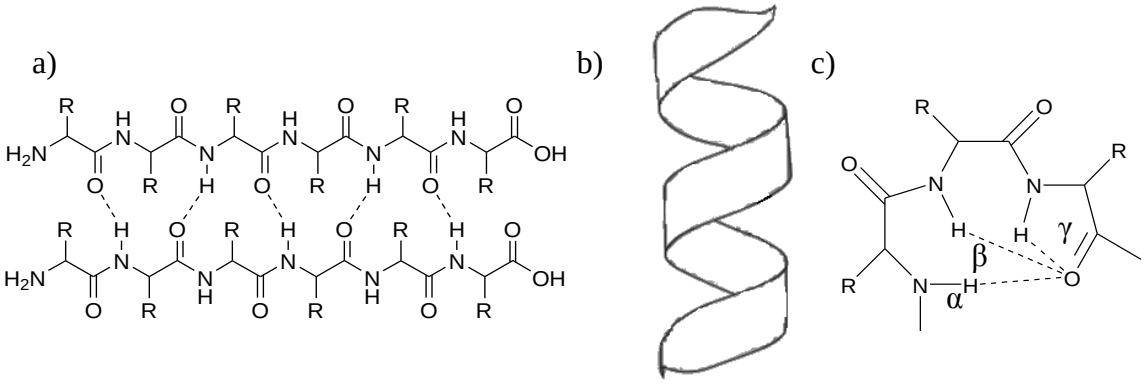

Figure 1.4. a) β-sheet showing hydrogen bonding between strands b) α-helix, hydrogen bonding is on the outside of the helix with every 4th amino acid hydrogen bonded c) α, β, and γ turns where hydrogen bonding is between amide and carboxyl group of opposite side of the turn

In contrast to the "normal" linear peptide chains that are formed by amide bonds, there is the possibility of forming cyclic peptides or cyclopeptides. Cyclopeptides occur when the amine and the carboxyl of the same peptide form an intramolecular amide bond that leads to ring closure. The properties, structure, and synthesis of both naturally occurring as well as synthetic cyclopeptides will be discussed in the next section.

1.2 CYCLOPEPTIDES

The conventional picture of a protein is series of amino acids in a linear chain with a number of secondary elements giving rise to both structure and properties. While this is an accurate description for most proteins, there have been recent discoveries on the

presence of cyclic proteins. There have been discoveries of cyclopeptides occurring in sources of plants, bacteria and even some animals,[3] which range in size from 14[4] to 78[5] amino acids in size. Figure 1.5 shows three isolated cyclopeptides from mammalian, plant, and bacterial sources.

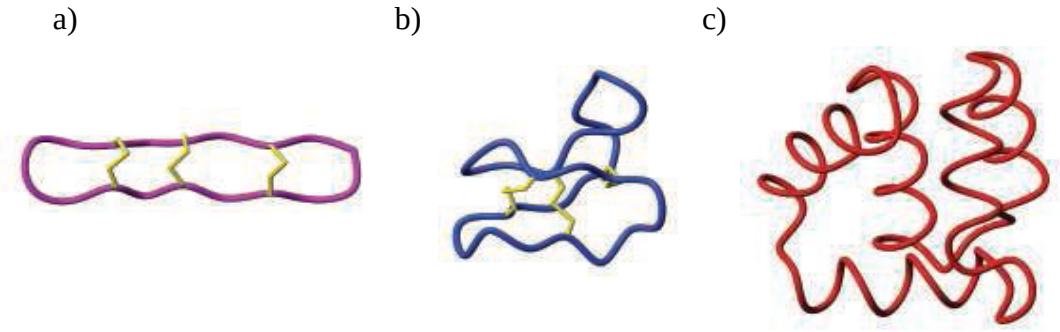

Figure 1.5 Cyclopeptides and small cyclic proteins isolated from bacterial, plant and mammalian sources. The structures shown were obtained by solution NMR studies. a) Protein rhesus θ-defensin–1 isolated from macaques monkeys. Three disulfide bonds in this small cyclopeptide give it both stability and rigidity. b) Cyclotide protein kalata B1 isolated from the plant Oldenlandia affinis. c) AS-48 bacterial protein isolated from Enterococcus Faecalis is currently being test as a food additive as well as uses in veterinary medicine as an anti bacterial protein.[6,7]

Cyclopeptides have inherently different properties compared to their linear peptide counterparts. For example, their hydrolytic stability has been shown to be greater.[3] While degradation of natural proteins happen by enzymatic reactions using a number of exopeptidase enzymes, cyclopeptides do not contain an amino or carboxy terminal side for exopeptidase (aminopeptidases or carboxypeptidases) to attach, therefore degradation by exopeptidases does not occur to cyclic peptides.[7] In addition cyclopeptides differ in their stability to extreme temperatures and pH.[7] Research has shown that bioactivity is still present in bacteriocin AS-48 at its biologically active

temperature after being exposed to temperatures near 93°C,[8] this is significantly higher than most linear proteins whose biological activity ceases at roughly 50°C. The activity is preserved because of the ability of the cyclic peptides to fold back into the active state, while linear peptides will deform and cannot refold into its active form. As well as the increased stability of cyclopeptides they have also shown to increase resistance to a number of disease and infections, most notably HIV.[9] Figure 1.6 shows the chemical sequence of rhesus θ-defensin–1 isolated from a macaque monkeys which has shown resistance to HIV. One of the most interesting features of cyclic peptides is their potential antibacterial properties. It is believed that cyclic peptides are able to incorporate themselves into the bacterial membrane, thus disrupting the membrane and decreasing or destroying the bacteria.[10] By combining both stability, as well as the increased activity seen in cyclopeptides, new drugs are now being designed to exploit these characteristics.[11,12]

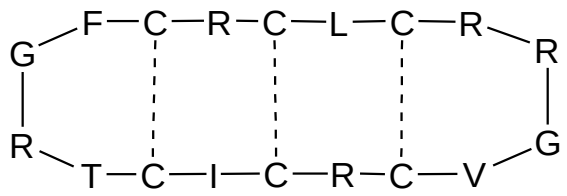

Figure 1.6 Chemical sequence of rhesus θ-defensin–1 isolated from macaques[13]. The HIV resistance protein has directed research to synthesis of cyclopeptide drugs because of their inherited stability. Three disulfide bonds are formed through six cysteine residues giving increased stability and rigidity.

When discussing cyclopeptides it is important to note that the largest number isolated has been from plants. Plants may contain a large number of cyclic peptides because of the harsh conditions they are subjected to as well as the large number of bacteria that can be present. These cyclopeptides, or cyclotides, are described as their

own subclass. The requirements of a cyclotide are a head-to-tail cyclization as well as disulfide bonds resulting in an increased stability and in many cases knotted topological structures.[14] Cyclotides are believed to have antibacterial, uterotonic, as well as have other biological activities.[14] Although the mechanism of how cyclic peptides act in biological systems is still unknown, it is believed that they disrupt cellular membranes. Kalata B1 protein, which has been administrated as a tea by an African tribe in the Congo for centuries,[7] has shown an affinity to bind to the membrane of bacteria. This binding is believed to be the mechanism of disruption to the cellular membrane.[15]

While the properties of cyclopeptides have been understood for a number of years, the biosynthetic pathway is often less known.[7] Although there have been advancements in the understanding of gene coding for cyclopeptides, there is still much to learn about the enzymes that are present during formation.[7] The leading theory in cyclopeptide formation is that in a linear chain protein, the section that is to be cyclized will be cut by an enzyme, which can then either pass off the peptide to another enzyme for cyclization or may cyclize the peptide itself.[3] Because the cyclic structure of the proteins are encoded in the genes that form these proteins, gene "grafting" can be used to easily synthesis potential highly active drugs.[16] Other then gene grafting studies on cyclopeptides there has also been synthetic research to cyclopeptides.[17-21]Cyclization of peptides with varying results of both yield and purity has been reported using many different techniques. Microwave radiation,[13] metal template assistance,[17] anion templating,[18] and solid phase synthesis[21] (Figure 1.7) are examples of techniques used for cyclic peptide synthesis.

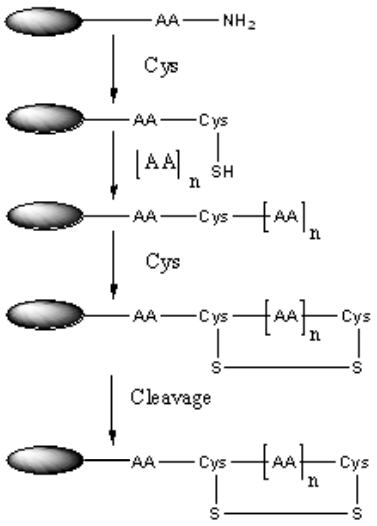

Figure 1.7 Synthetic scheme for solid phase synthesis of a cyclic peptide redrawn from reference16. Disulfide bonds are formed between cystein residues to form the cyclized product.[21]

Using a chemical synthetic approach it is possible to incorporate other non-natural groups into the sequence that add functionalities and properties such as metal coordination sites or the ability to form larger more complex structures. Examples of these cyclic pseudopeptides were made by addition of pyridine into a cyclic peptide for metal binding,[22] an addition of a ferrocene (Fc) group for redox properties and to control the self-assembly properties of the conjugate,[23] and substitution of a trifluoromethyl group which changes the interactions to studied enzymes (Figure 1.8).[24]

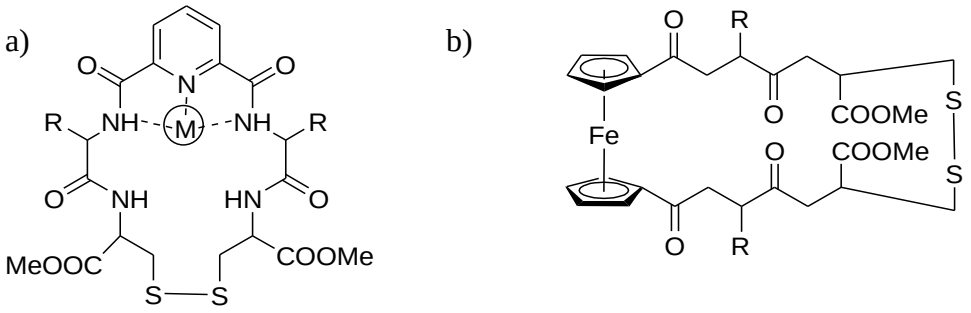

Figure 1.8. a) Example of how the addition of pyridine into the cyclic peptide allows for metal binding redrawn from reference 22 b) Structure of a cyclic peptide containing a ferrocene group redrawn from reference 23.

1.3 TOPOLOGICALLY LINKED MOLECULES

Webster's dictionary defines topology as "the study of geometric configurations that are unaltered by elastic deformations."[64] With this being the definition of topology, topologically linked molecules can then be described as two or more independent interlocking molecules that cannot be unaltered by elastic deformations. In the field of chemistry there are two main classes of topologically linked molecules that will be discussed in this thesis. The first is the catenanes, which can be seen in Figure 1.9a. A catenane consists of two or more interlocking rings that cannot be separated without breaking a covalent bond. The second class to be discussed is the rotaxanes (Figure 1.9b). A rotaxane is described as a cyclic compound that has a linear component running through the center of the ring which is then "stoppered" at either end preventing the macrocycle from slipping off the linear portion. Topologically linked molecules have been studied in areas of biology as well as material science each of which will be discussed briefly.

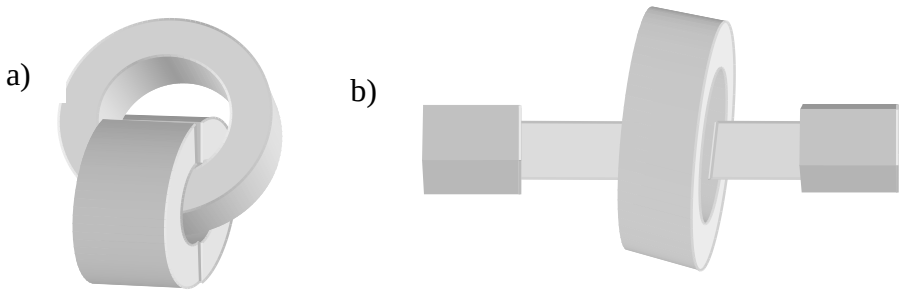

Figure 1.9. a) Drawing of a catenane where both rings are interlocked with each other. b) Drawing of a rotaxane where the linear string goes through the center of the cyclic component then is capped on either end.

1.4 OBJECTIVE AND APPROACH

The objective of research described in this thesis is to prepare cyclic peptide conjugates that contain both ferrocene (Fc) and diphenol phenanthroline (Dpp) moieties. Such systems are not known to date and may exhibit interesting properties such as metal binding as well as redox properties. Research in this thesis will describe my results in this area.

The Fc group is a well known and studied redox probe[25,26] which is also known to specific secondary structures into the conjugate, such a turn-motif. In addition, the Fc group will guide and control the hydrogen bonding interactions between the peptide substituents.[27,28] The Dpp group has turn inducing properties,[29] it can complex metals, and has the potential to induce π interactions with adjacent Dpp groups that can lead to interesting supramolecular arrangements of the molecules in the solid state.[30] In this thesis, results will be presented that are related to these issues and will show the roles of Dpp and of the peptide for the self-association of the molecules in the solid state.

During the synthesis of cyclic compounds there are a number of problems that can occur and need to be addressed. The order, the speed, and the dilution of the reaction mixture will all influence the outcome of the reaction, including the yield of the desired cyclic product. Polymerization of the peptide is the leading concern during cyclization reactions and occurs when the kinetics of the intermolecular reaction is faster than that of the cyclization. In any cyclization reactions, mixtures of dimers, trimers and larger oligomers will be formed, as well as open chain polymers of increasing chain length. The goal of the cyclization reaction is to control any side product reactions so that the desired cyclic product is obtained in the highest yield possible. This can be achieved in a number of ways. Ring closing metathesis,[31] templating,[32] high dilution[28] and complexation[33] are four techniques that have been described in the literature and that have given good results. For the cyclization reactions that were preformed in this thesis high dilution was combined with slow addition of the reactants.

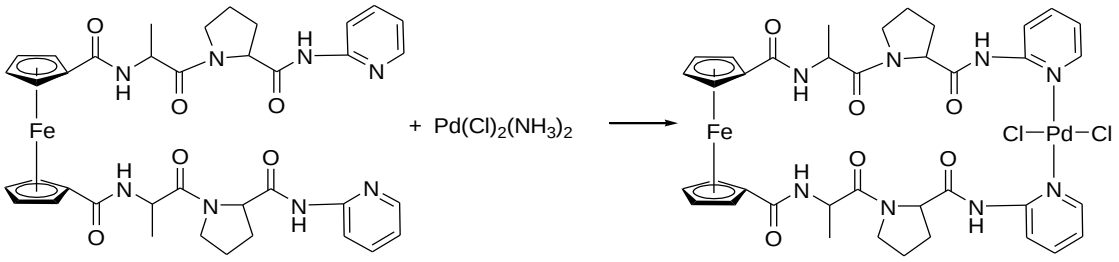

Figure 1.10. Cyclization of ferrocene dipeptide using metal complexation from reference 31 in DCM.

The approach to the synthesis of cyclic peptides for this thesis will be first coupling a series of amino acids (AA) to Dpp through an ester linkage using DCC/DMAP. This will allow a series of new Dpp-AA compounds to be reported as well as metal complexation studies can be done. The next step in cyclization will be

deprotection of Boc and cyclization using ferrocene diacetyl chloride ($Fc[COCl]_2$) at high dilutions and slow addition. The acid chloride was selected because of its reactivity with the amino group of amino acids. Using the acid chloride method for amide bond formation does not require the use of coupling reagents, such as carbodiimides. As new compounds are synthesized they are characterized by nuclear magnetic resonance (NMR), mass spectrometry (MS), x-ray crystallography and electrochemical studies if a redox probe is present.

CHAPTER 2.

NOVEL CYCLIC DIPHENOL PHENANTHROLINE COMPOUNDS

As a first step in this investigation, it was necessary to examine the possibility of preparing phenathroline amino acid, peptide, and ferrocene conjugates. This chapter focuses on the preparation and the properties of such conjugates.

2.1 RESULTS AND DISCUSSION

Diphenol phenanthroline (Dpp) was used to examine the possibility of controlling supramolecular systems created by π- π stacking. The first compound synthesized was Dpp coupled to ferrocene through an ester linkage. There are two common methods for ester formation in literature: the Steglich reactions using DCC/DMAP and the acid chloride method. Both approaches were tested.[34,35] The first attempt at synthesizing Fc-Dpp (**1)** with DCC/DMAP did not yield the desired product. Probable difficulties could have arisen by the possibility of polymerization during cyclization as well as inactive urea side products may have been formed. Next the acid chloride approached was tested, the synthesis was carried out via refluxing equimolar amounts of ferrocene dicarboxylic acid chloride and Dpp in dichloromethane as shown in Scheme 2.1

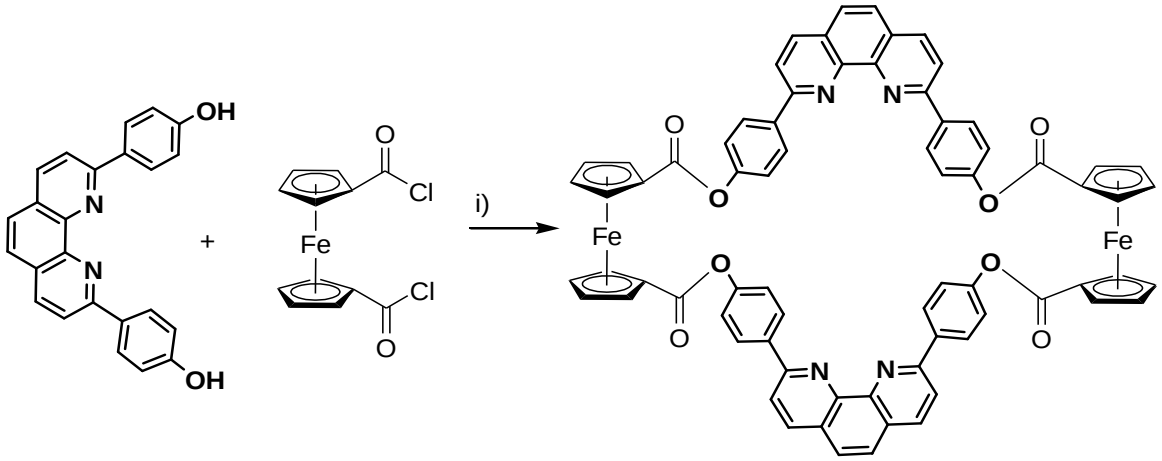

Scheme 2.1 Synthesis of $[Fc\text{-}Dpp]_2$ using the acid chloride method. Equimolar amounts of $Fc[COCl]_2$ were reacted with Dpp in dichloromethane giving the desired dimer $[Fc\text{-}Dpp]_2$ (**1**) in 5% yield. i) Reflux in DCM

The crude product was purified by column chromatography on silica using 1% TEA in ethyl acetate as the eluant with an R_f of 0.2. The isolated compound **1** is poorly soluble which complicated the purification. Compound **1** was examined by ^{1}H-NMR in $CDCl_3$. There is a plane of symmetry bisecting the molecule and this is observed as equivalent peaks in the NMR spectrum Figure 2.1. Minor impurities and line broadening are observed in the NMR spectrum.

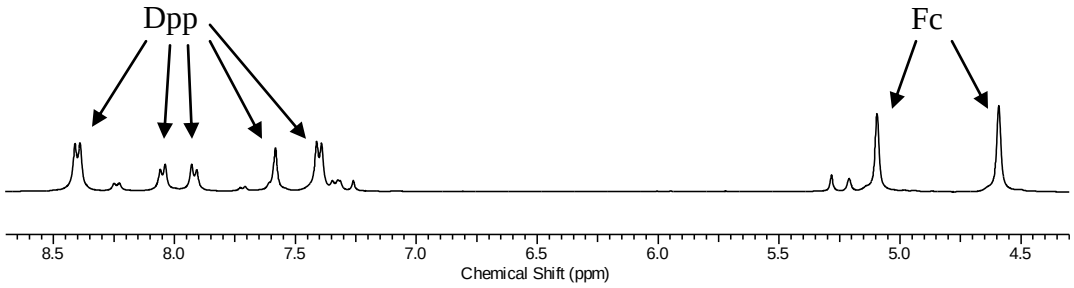

Figure 2.1. ^{1}H NMR of $[Fc\text{-}Dpp]_2$ (1). Aromatic protons of Dpp are observed in the range of δ 7.3 to 8.4. Symmetrical Fc protons are observed as two singlets at δ 4.52 and 5.10.

^{13}C NMR spectroscopy was attempted on $[Fc\text{-}Dpp]_2$. However, due to its low solubility and its ease of precipitation, I was unable to acquire reasonable high quality ^{13}C NMR spectra. Different solvents were tired but all were found to precipitate the compound further. Mass spectrometry was carried out by electro spray ionization (ESI) giving a M+ peak at m/z = 1205 suggesting the presence of the symmetrical dimer. To gain further insight single crystals were grown of compound **1** in the presence of a co-crystallizing solvent. Figure 2.2 shows the x-ray structure of $[Fc\text{-}Dpp]_2$ **1** with four molecules of chloroform which was solved by Gabrielle Schatte, U of S. Selected bond distances and angles are listed in Table 2.2.

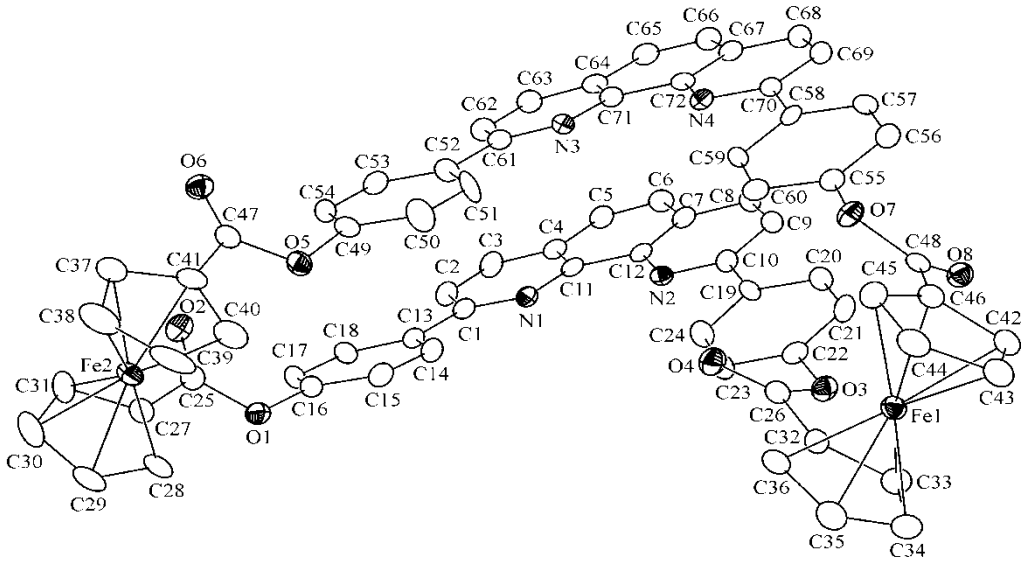

Figure 2.2. ORTEP drawing of compound **1**. All hydrogen atoms and four chloroform molecules are omitted for clarity. All crystallographic parameters are summarized in Table 2.1.

The crystal structure shows that the two phenanthroline rings are planar, while the four phenol rings are slightly bent out of the plant with respect to the phenanthroline as indicated in Figure 2.3. The two phenanthroline rings engage in π stacking interactions with distances ranging from 3.81Å for the A-A` distance to 4.02Å for the D-D` distance. (Figure 2.3b) These distances are in the range reported for phenanthroline π-π stacking.[36] The observed offset between the two phenanthroline rings has also been seen before, and is described by Umezawa et al. This offset increased the π-π interactions and stabilizes the system.[37] Figure 2.4 shows a top down view looking through both Fc groups, which shows that both Fc units are nearly eclipsed having the substituents in a 1,1'-configuration. In the absence of hydrogen bonding interactions proximal to the Fc group there is no preferred orientation of the carbonyls on the Fc groups.

Table 2.1. Crystallographic data	**1**	**3**
Empirical formula	$C_{76}H_{48}Cl_{12}Fe_2N_4O_8$	$C_{62}H_{68}Cl_6FeN_6O_8$
Formula mass	1682.28	1293.77
Crystal color, habit	orange, plate	yellow, plate
Crystal dimensions [mm]	0.08 × 0.08 × 0.05	0.30 x 0.25 x 0.10
Crystal system	triclinic	Orthorhombic
Space group	$P\bar{1}$ [No. 2]	P212121
Unit cell parameters:		
a [Å]	15.0222(8)	17.4544(6)
b [Å]	15.6770(7)	17.9342(5)
c [Å]	16.7177(10)	20.5922(9)
α (°)	101.871(3)	90.00
β (°)	98.999(3)	90.00
γ (°)	108.073(3)	90.00
V [Å3]	4079.36(13)	6446.0(4)

Z	2	4
F(000)	1704	2696
ρcalcd. [Mg/m3]	1.570	1.333
μ [mm]	0.919	0.539
Radiation (Å)	Mo-*K*α λ = 0.71073	Mo-*K*α λ = 0.71073
Temperature [K]	173(2)	150(2)
θ range for data collection [°]	3.18-22.98	2.55 to 21.96
Total reflections	17113	44228
Independent reflections [*F*o2 _ 3σ(*F*o2)]	9822(*R*int = 0.0692)	7870 [R(int) = 0.0640]
Observed reflection [*F*o2 _ 2σ(*F*o2)]	6400	44228
Data/restraints/parameters	9822/1266/955	7870/758/747
Absolute structure parameter	–0.020(18) (1457)	0.09(6)
S (Goodness-of-fit on *F*2)	1.010	1.136
Final *R* indices:		
*R*1[a] [*I*o _ 2σ(*I*o)]	0.0614	0.1152
*wR*2[b] (all data)	0.1464	0.2590
Largest difference peak/hole [e– Å3]	1.140 and -.0884	.0714 and -.454

Table 2.2. Selected bond distances (Å) and angles (°) for $[FcDpp]_2$ (**1**)

Bond Distances	**1**
O(4)-C(26)	1.201 (6)
O(8)-C(48)	1.207 (6)
O(2)-C(25)	1.195 (7)
O(6)-C(47)	1.192 (7)
Av Fe(1) CCp	2.050 (6)
Av Fe(1) CCp`	2.047 (6)
Av Fe(2) CCp	2.034 (7)
Av Fe(2) CCp`	2.039 (6)
Bond Angles	
O5-C47-C41	109.6 (5)
O1-C25-C27	110.2 (5)
O3-C26-C32	110.7 (5)
O7-C48-C46	111.1 (5)
O6-C47-O5	124.3 (5)
O6-C47-C41	126.1 (5)
C71-N3-C6-C52	180.0 (5)
C11-N1-C1-C13	175.6 (4)
C12-N2-C10-C19	178.6 (4)
C72-N4-C70-C58	174.9 (4)

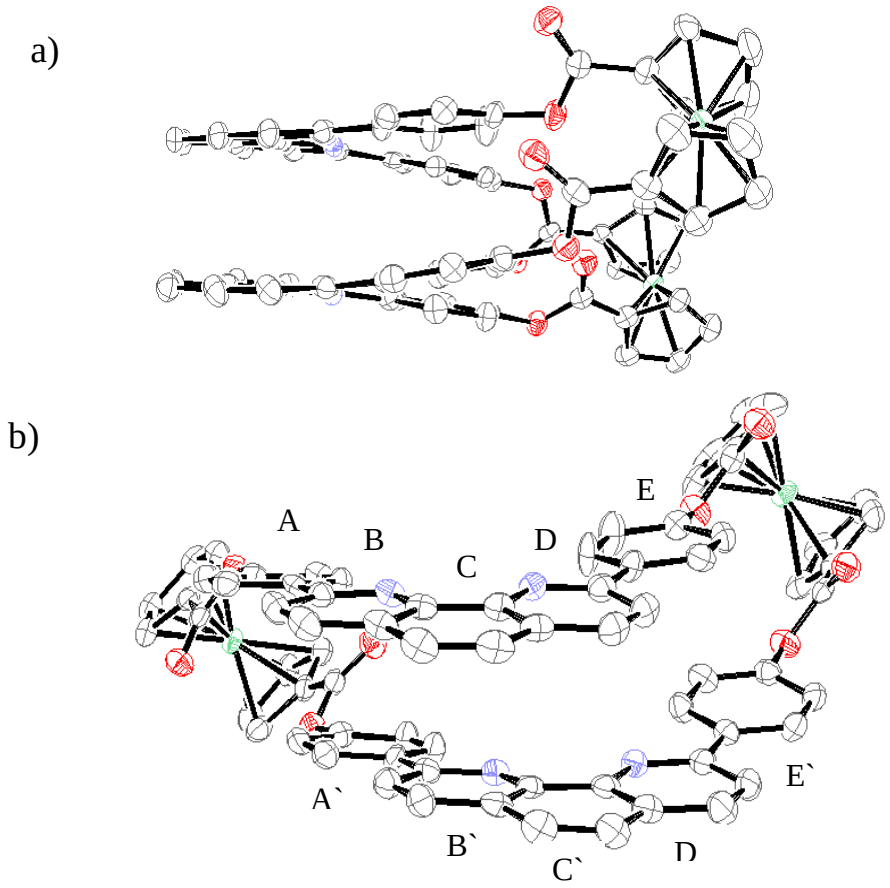

Figure 2.3. Molecular structure of compound **1**. a) Side view showing the phenanthroline system in the plane. b) End on view with phenanthroline rings stacked over each other with π-π stacking. A`-E` denotes the bottom ring of π-π stacking. Distances are given in Å. A-A' = 3.81, B-B' = 3.99, C-C' = 3.85, D-D' = 4.02, E-E' = 4.02. The top ring is slightly offset to the left with respect to the bottom ring, resulting in stronger π interactions between the aromatic systems.

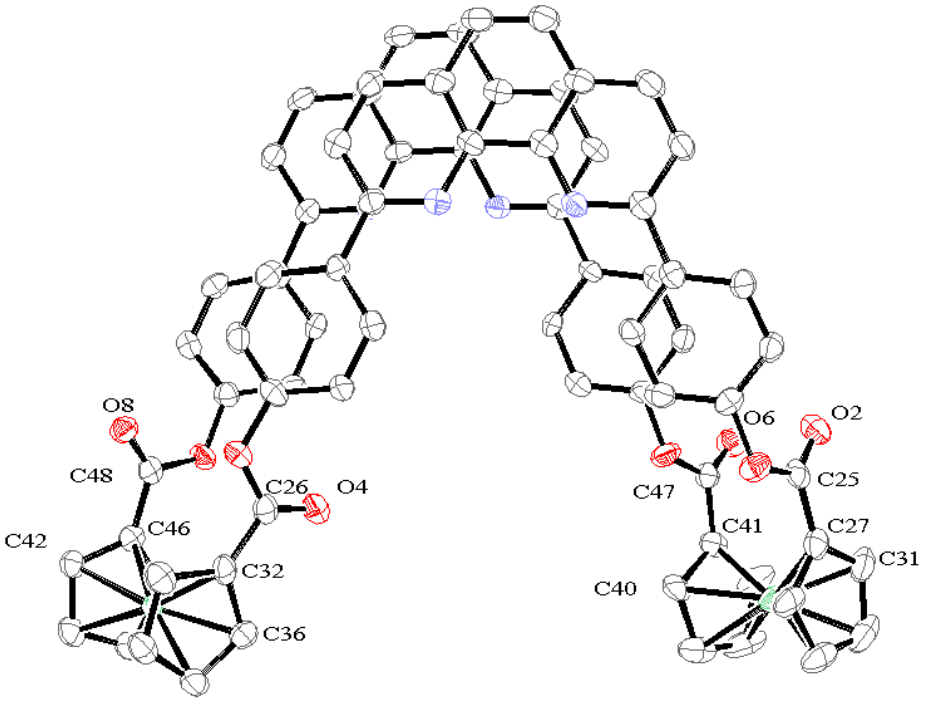

Figure 2.4. Bottom ferrocene is in E,E conformation while the top ferrocene is in Z,E conformation. Torsion angles are given in °. C36-C32-C26-O4 = 3.80°, C42-C46-C48-O8 = 7.79°, C31-C27-C25-O2 = 4.71°,C37-C41-C47-O6 = 7.01

This leads to having two different rotational isomers, one being E,E and the other being Z,E, indication the relative mixture of the carbonyls on the Fc groups with respect to each other. In the E,E isomer both carbonyls are facing out of the molecule, while in the Z,E isomer the top ring carbonyl is facing in (Z), while the bottom ring carbonyl is facing out (E). Torsion angles between the Cp rings and the proximal carbonyls are in the range of 3.8 to 7.8°. With such small torsion angles for the carbonyls, the interactions between Fc and the carbonyls with respect to electronic communication will be high because of their π orbital overlap.[38] Crystal packing of **1** reveals short contacts between the H atoms of the Cp rings and the π systems of the phenanthroline. Such weak C(H)-π interactions were observed before and are often significant in that it influences the

packing of the molecules in the solid state (Figure 2.5a) .[30] The intermolecular interactions of compound **1** are determined by CH-π interactions and not the π-π interactions.

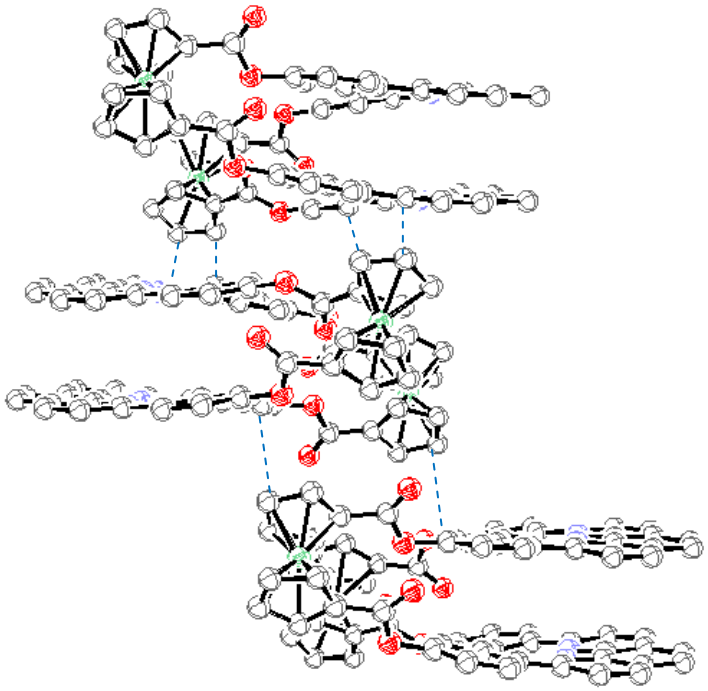

Figure 2.5. a) A view down the C axis of compound **1**. Blue lines indicating CH-π interactions from Cp rings of ferrocene and the phenanthroline π system in the crystal packing. C(H)···π = 3.36Å, C(H)···π = 3.35Å.

Thus the π systems do not stack one on top of each other but instead the packing is best described as head to tail. There are two different distances for the CH-π interactions, 3.35 and 3.36Å, these are within the range reported earlier for other CH-π interactions.[30] Similar packing between Fc-CH and phenanthroline has been seen before for similar systems.[39] The actual packing of the system in reference 39 is not discussed in

great detail but it is apparent that the packing of the system is not between π interactions but instead between Fc and π interactions. Figure 2.6 shows the single unit of 1,1'-Bis{[4-(1,10-phenanthroline-3-yl-ethynyl)-2,5-dipropoxyphenyl] ethynyl}ferrocene in which the single crystal structure is determined by π stacking, while the packing is determined by Fc CH-π interactions. The single unit shows π stacking between the phenanthroline units at distances of 3.360-3.469Å which is slightly smaller then the distances seen for compound **1.** This can be justified by the flexibility in the system allowing for the phenanthroline to be tighter packed.

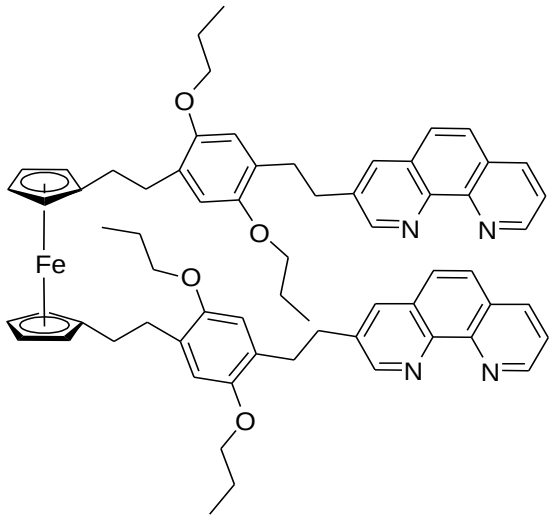

Figure 2.6. Single unit of 1,1'-bis{[4-(1,10-phenanthroline-3-yl-ethynyl)-2, dipropoxyphenyl] ethynyl}ferrocene. The two phenanthroline units overlap leading to π-π interactions in the single unit, while the packing of the system is a zig-zag pattern where the CH of Fc interacts with a neighboring phenanthroline.[39]

The next step was to examine the synthesis Fc and Dpp containing macrocycles in which peptide spacers separate the Fc and Dpp groups. (Scheme 2.2). It is believed that peptide spacers will enhance both intramolecular and intermolecular interactions, and one might assume that a balance will be struck between intramolecular hydrogen bonding of the peptides and the π stacking of the aromatic groups. A number of amino acids were

inserted as linkers between the Dpp and Fc giving many new properties to the macrocycles. By inserting amino acids we introduced and examine significant intermolecular H-bonding interactions, increase the solubility of the macrocycle, as well as increase the size of the macrocycle in hopes of synthesizing the monomer. The first step in this synthesis was to couple di-leucine, tri-leucine, glycine, and leucine-alanine to Dpp using DCC/DMAP coupling reagents giving the corresponding bis-substituted Boc protected Dpp-amino acid conjugates **2**, **4**, **6**, and **7** (Scheme 2.2).

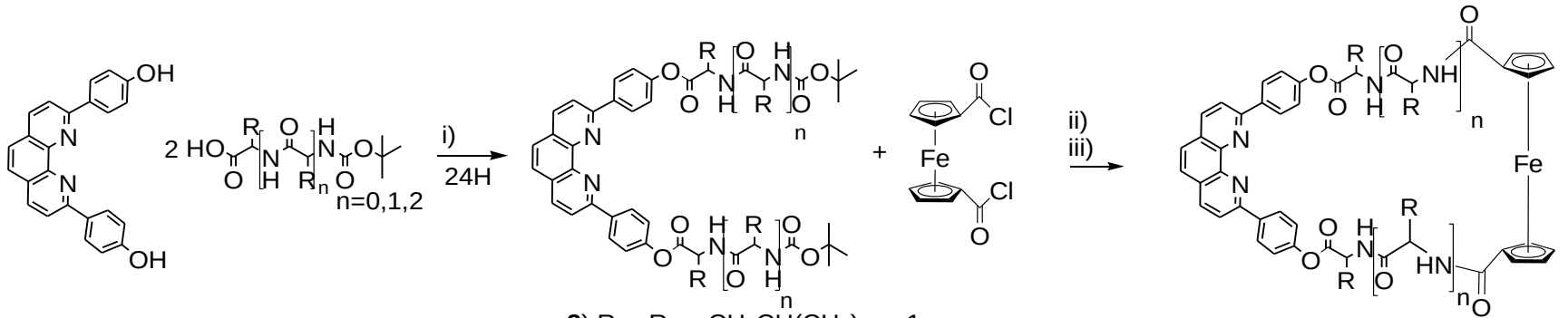

2) $R_1 = R_2 = CH_2CH(CH_3)_2$ n=1
4) $R_1 = R_2 = CH_2CH(CH_3)_2$ n=2
6) $R_1 = R_2 =$ H n=0
7) $R_1 = CH_2CH(CH_2)$ $R_2 = CH_3$ n=0

3) $R = CH_2CH(CH_3)_2$ n=1
5) $R = CH_2CH(CH_3)_2$ n=2

Scheme 2.2. Reaction scheme for compounds **2-7**. i) DCC:DMAP/DCM, ii) TFA/DCM, iii) TEA/DCM. **2,4,6,7** are bis-substituted Dpp-AA compounds synthesized by ester formation using23 DCC/DMAP coupling reagents. The desired Fc-conjugates **3** and **5** are synthesized by high dilution cyclization from the protected Boc-peptide Dpp conjugates **2** and **4.**

Compounds **3** and **5** were then obtained after deprotecting compounds **2** and **4** using trifluoroacetic acid (TFA) to remove the Boc group, followed by slow addition of $Fc[COCl]_2$ at high dilution, followed by purification by column chromatography to give the desired compounds **3** and **5** in 8 and 9% yield, respectively (Scheme 2.2). A sample ^1H NMR of compound **6** is shown in Figure 2.7.

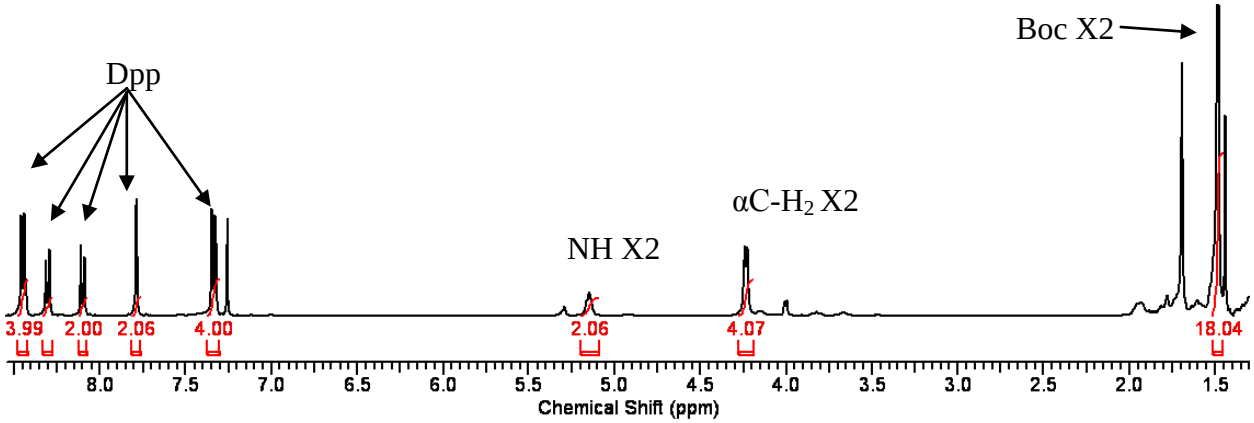

Figure 2.7. ^1H NMR spectrum of $Dpp(Gly\text{-}Boc)_2$ (**6**) in $CDCl_3$.

Single crystal diffraction studies of compound **3** were carried out by Michael Jennings at UWO. The ORTEP drawing of compound **3** is shown in Figure 2.8. A summary of the x-ray data is provided in Table 2.1. Selected distances and angles are reported in Table 2.3. It is important to point out the positional disorder in the distal carbonyls, in which the E,E conformation is present in a twofold amount compared to the Z,E conformation. The exact ratio for the two conformations is 63:36% or approximately 2:1. The single unit crystal of **3** shows the predicted intramolecular hydrogen bonding between amide and the opposite Leu C=O, resulting in a 10-membered hydrogen bonding pattern has been observed before for similar ferrocene peptide conjugates,[28] and is now known as the "Herrick pattern".[40]

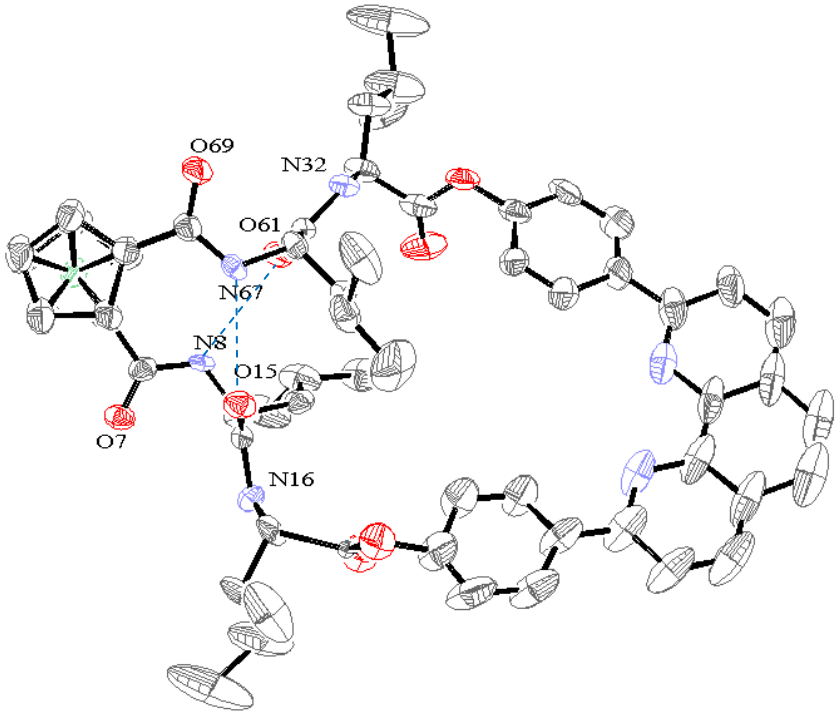

Figure 2.8. ORTEP of **3.** The ferrocene is in a 1,2'-P helical conformation with both proximal carbonyls in E,E conformation and two intramolecular hydrogen bonds shown in blue. N(67)···O(15)=3.06Å, N(8)···O(61)= 3.06Å. All crystallographic parameters are summarized in Table 2.1.

Table 2.3. Selected bond distances (Å) and angles (°) for $[Fc[Leu_2]_2Dpp]_2$ (**3**)

Bond Distances	**3**
O(7)-C(6)	1.259 (14)
O(69)-C(68)	1.229 (14)
O(15)-C(14)	1.204 (13)
O(53A)- C(52A)	1.30 (2)
O(53B)- C(52B)	1.08 (4)
Av Fe(1) CCp	2.047 (14)
Av Fe(1) CCp`	2.041 (14)
Bond Angles	
O(7)-C(6)-C(5)	120.4(11)
O(69)-C(68)-C(70)	119.8(11)
O(7)-C(6)-N(8)	120.8(10)
O(7)-C(48)-C(46)	111.1 (5)
O(6)-C(47)-O(5)	124.3 (5)
O(6)-C(47)-C(41)	126.1 (5)
O(7)-C(1)-C(5)-C(6)	175.6(12)
O(69)-C(68)-C(70)-C(71)	173.2(12)
C(34)-N(35)-C(36)-C(45)	177.0(12)
C(33)-N(32)-C(31)-C(28)	174.6(13)

The supramolecular structure for **3** is controlled by intermolecular hydrogen bonding between the proximal carbonyl of ferrocene to the opposite molecule's amide of the second amino acid from ferrocene. There are however, no π-π interactions between the phenanthroline groups of adjacent single units. Figure 2.9 shows how three units are linked head to tail via hydrogen bonding involving the Fc-CO and the amide NH proximal to the phenanthroline of an adjacent molecule. The resulting strand pattern is a alternating 10 and 14-membered H-bonded repeat along the strand. This alternating 10 and14 membered hydrogen bonding pattern resembles that of a antiparrel beta sheet and has been discussed before for other ferrocene peptide conjugates.[41,42] The 10-membered ring can be seen by counting the atoms in the intramolecular hydrogen bonding, while the 14-membered ring is seen by the intermolecular hydrogen bonding. The distance of 3.06Å for the intramolecular hydrogen bonds and distances of 2.81-2.84Å are both nearly identical to those reported earlier for other ferrocene beta sheets, 3.06Å for intramolecular and 2.87Å for intermolecular. Figure 2.9b shows a drawing of an antiparrellel beta sheet that shows the 10-14 hydrogen bonding that is seen in figure 2.9a.

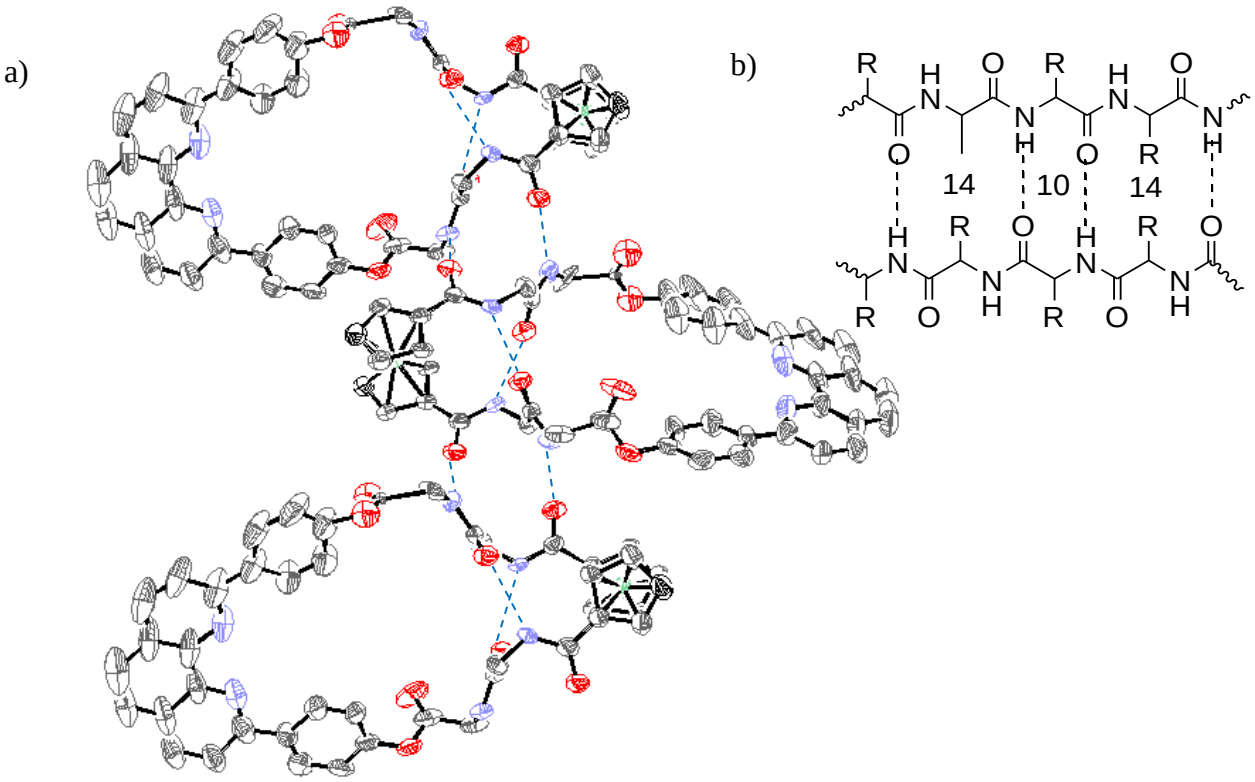

Figure 2.9. a) Three units of **3** with leucine side chains removed for clarity, showing intra and intermolecular hydrogen bonding with head-to-tailassembly of Fc-peptide-Dpp conjugates. Selected intermolecular hydrogen bonds distances: N(59)···O(7') = 2.81 Å N(16')···O(69) = 2.84 Å. b) Drawing of an antiparrallel β-sheet showing alternating 10- and 14-membered rings.

Figure 2.10 shows the interaction of strands of **3** with C(H)-π interactions between the strands which are shown in Figure 2.9. Distances of 3.1-3.3Å are observed for these interactions, much like the interactions observed for **1** which determined the packing. Although there are a number of hydrogen bonds present in compound **3** between the amide and carbonyl as well as the C(H)-π interactions, there are no π-π interactions between the phenanthrolines of adjacent molecules.

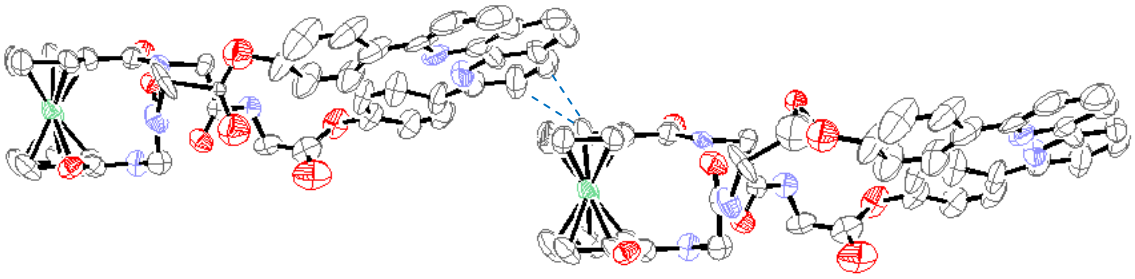

Figure 2.10. X-ray structure of compound **3** showing C (H)-π interactions between hydrogen bonded strands shown in figure 3.0. Leucine side chains have been removed for clarity. C (H)···π = 3.13 Å and 3.27

In similar systems where there is both the ability to hydrogen bond (N-H···O) as well as π stack, the leading factor in the packing of the crystal structure is the hydrogen bonding.[41] Figure 2.11 shows the drawing of 3-bromo-N-(2-hydroxy-1,1-dimethylethyl)benzamide which reported both π-π interactions at distances of 3.54Å as well as hydrogen bonding at distances of 1.92, 2.35, and 2.38Å. .

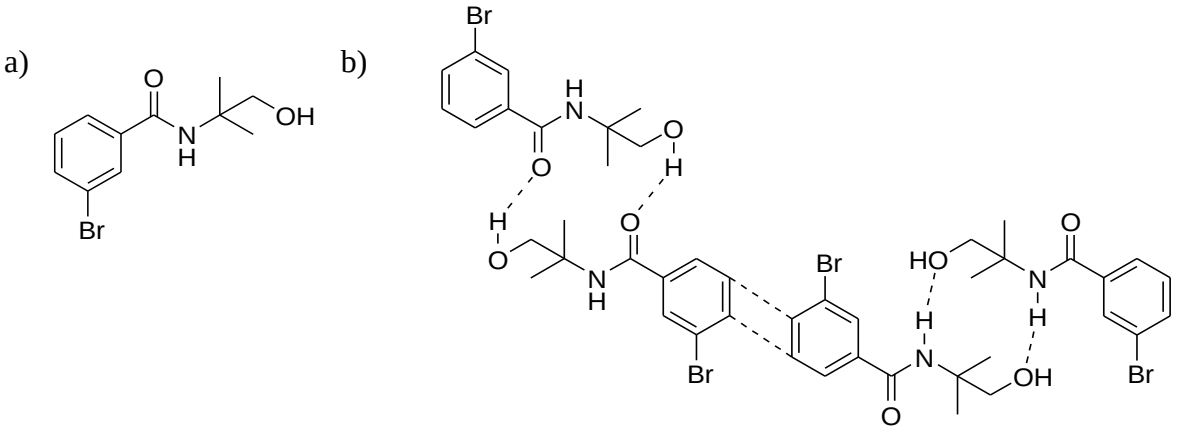

Figure 2.11. a) Drawing of 3-bromo-N-(2-hydroxy-1,1-dimethylethyl)benzamide. Interactions between aromatic ring are observed as well as hydrogen bonding. The overall crystal structure is a combination of both.[41] b) Packing of 4 single units. Hydrogen bonding and π-π stacking is shown with dashed lines. π-π interactions are 3.54Å while the three different hydrogen bonds are 1.92, 2.35, and 2.38Å.

The hydrogen bonding is believed to be the leading factor to the crystal packing, with π stacking forming once the single molecules are aligned with all possible hydrogen bonds first formed. When this is added to the fact that Fc-CH is able to interact with π systems it is apparent that the overall packing of the system is a combination of both hydrogen bonds as well as CH-π interactions but is not controlled by π-π interactions. By looking at the energies associated with each of the different bonds it can be seen that there is a conservation of a small amount of energy with hydrogen bond formation over π stacking. Using the computational number of 1-1.5 kcal/mol[42] for π-π interactions and 1-5kcal/mol[43] for amide hydrogen bonding, it can be seen that there is the possibility for a lowering of energy with an increased number of hydrogen bonds. It also needs to be noted that the crystals were grown in nonpolar solvents which would allow more intermolecular hydrogen bonds.

Conclusion

In this chapter, the first series of cyclic ferrocene phenanthroline amino acid and peptide conjugates were prepared and studied in solution and the solid state. The peptide conjugates engage in intermolecular H-bonding and exhibit C-H π interactions resulting in the formation for larger supramolecular assemblies. In the next chapter, the ability of phenanthroline peptide conjugates to complex metal ions is explored which is critical for the catenation and formation of rotaxanes.

CHAPTER 3.

DIPHENOL PHENANTHROLINE METAL BINDING

In this chapter, metal binding to the phenanthroline group is described. In particular, Cu^{+} and Zn^{2+} complexation to the Dpp group are studied by electrochemistry and mass spectrometry. Metal complexation is critical en route to peptide catenane formation.

3.1 METAL BINDING STUDIES

In the previous chapter, the synthesis of Fc-Dpp and Dpp-amino acid conjugates was described. In this chapter, studies aimed at elucidating the interactions of these conjugates with Zn and Cu ions will be done. These metal ions were chosen because of their known ability to form complexes with Dpp. In the case of Cu, complexation of Dpp conjugates with Cu(I) is facile and in fact is a synthetically useful method for the formation of catenanes. Hence, we explored this avenue – without too much success, as will be described in Chapter 5.

We studied the reaction of the macrocycle Dpp-Fc (**1**) with Zn^{2+} and a number of the Dpp-AA compounds (**2,4,6,7**) with Cu^{+}. For both systems, it is expected that metal binding takes place at the Dpp, as reported for other Dpp systems.[44,45] Figure 3.1 shows two phenanthroline metal complexes. The uses of metal chelation in the compounds shown in Figure 3.1 all use the metal ions for supramolecular building.

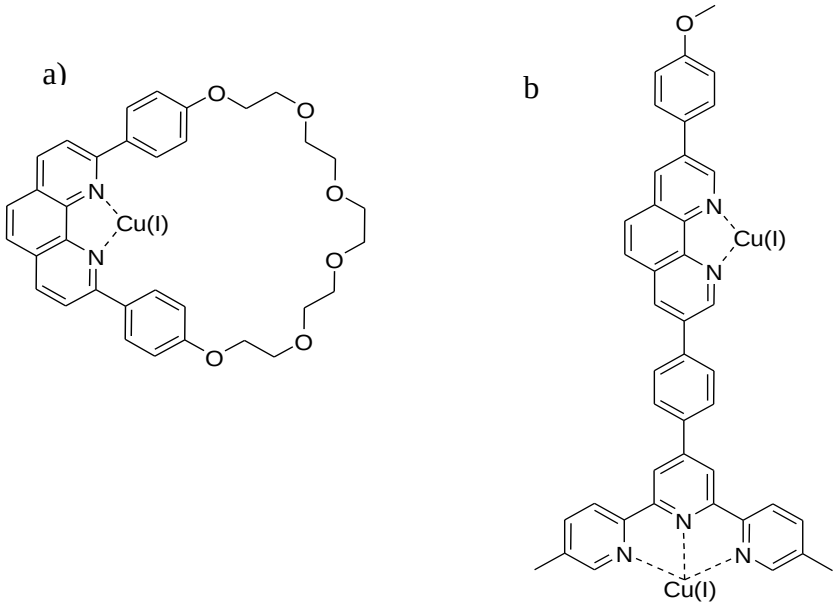

Figure 3.1. a) Drawing of a phenanthroline polyether macrocycle complexed to Cu(I).[44] b) Multi-chelate ligand that shows interesting 3D structures when complexed to metal ions in different ratios.[45]

By having phenanthroline in the compounds it is possible to predict and design 3-dimensional structures. The polyether macrocycle seen in Figure 3.1a has been used in catenane synthesis[44] while the phenanthroline compound in Figure 3.1b has been used as a building block for the generation of 3-dimensional structures.[45]

Metal chelation to the Dpp conjugates (**1,2,4,6,7)** was investigated electrochemically and in the case of the Dpp-peptide conjugates by mass spectrometry. Unfortunately, we were unable to obtain crystalline materials that were suitable to carry out structural investigations.

In the case of $[Dpp\text{-}Fc]_2$, it is expected that metal coordination to the Dpp ligand will cause an interference in the redox properties of ferrocene. Beer et al. has reported that there are five different mechanisms that can be present with the different types of complexes formed between a redox center and the complexed metal.

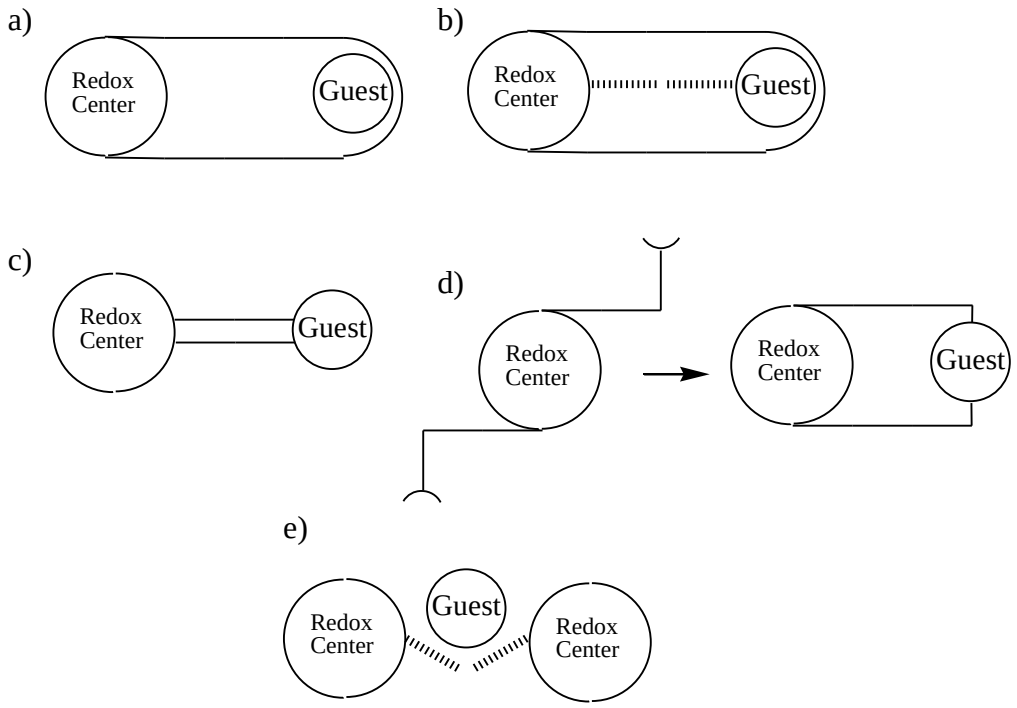

Figure 3.2. Five different mechanisms for coupling electrochemical and complexation reactions. a) Through space b) Bond linkage c) Direct coordination d) Change in conformation e) Presence of guest disrupts interaction. [46]

The five mechanisms are, through space, direct coordination, bond linkage, change in conformation and disruption interactions (Figure 3.2). [46] Of these five interactions the largest interference is seen when the redox center is both directly bonded to a metal as well in close proximity to allow through-space interactions. Figure 3.3a shows a ferrocene compound with two complexation sites which are directly connected to ferrocene through the amine. The resulting interaction between metal ions is a large anodic shift in the electrochemical properties. When a single Zn^{+2} is complexed a shift of +320 mV is observed and a larger shift of +720 mV is seen for two complexed Zn^{+2} ions.[47] A different type of interaction is seen for the compound in Figure 3.3b. This ferrocene bismacrocycle when complexed with K^{+} ions shows a cathodic shift in the $E_{1/2}$. This is rationalized by a conformational disruption that is thought to occur to allow the

K^+ ion to be sandwiched between the two macrocycles. This conformational change pushes electrons from the S atom onto the ferrocene group causing a cathodic shift of -60 mV.[48]

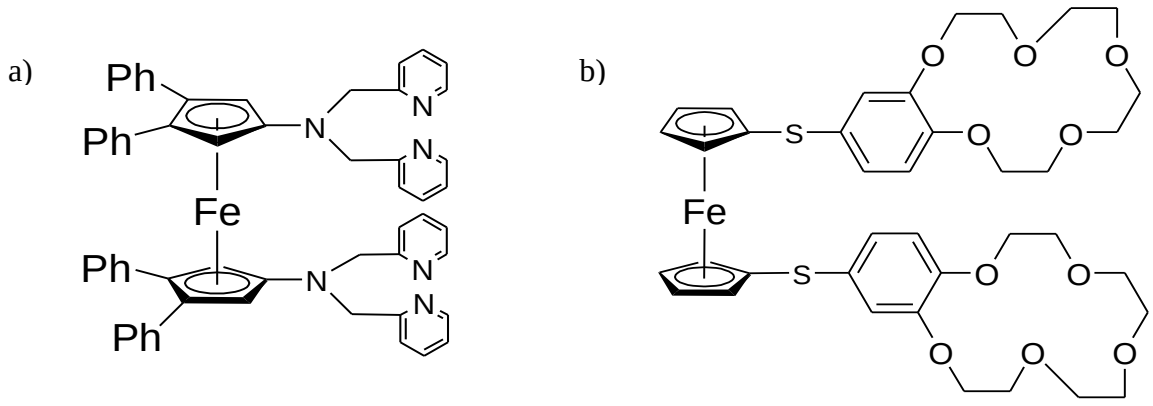

Figure 3.3. a) Ferrocene compound with two coordination sites. Electrochemical studies show that a cathodic shift is observed when metal ions are complexed.[47] b) Ferrocene bis-macrocycle that shows a cathodic shift of -60 mV when a K^+ is sandwiched between the two macrocycles.[48]

When Na^+ is complexed to the system, an anodic shift is observed, since coordination of the cationic Na^+ will make it more difficult to oxidize the Fc group. It is believed that due to the smaller ionic radius of Na^+ vs. K^+, there is no geometric distortion in the complex.

3.1.1 ELECTROCHEMICAL STUDIES OF [Fc-Dpp]$_2$ WITH Zn^{2+}

Using Dpp for the synthesis of cyclic molecules not only has the advantage of having π interactions to build the supramolecular framework but also the ability to chelate metal ions.[29] The interaction of the Fc-Dpp conjugate **1** with Zn^{2+} was studied in solution by cyclic voltammetry (CV). This approach should be highly sensitive for Zn^{2+} complexation and shifts in the halfwave potential $E_{1/2}$ should be observable. Figure 3.4

shows the CV of compound **1** in DCM and in a 2:1 mixture of DCM and ACN. The electrochemical parameters are summarized in Table 3.1. It is noticeable that the $E_{1/2}$ for compound **1** shifts cathodically as the solvent is changed from $E_{1/2}$ = 0.944 V to 0.877 V in a 2:1 solvent mixture. This potential shift is due to differences in Fc salvation and was observed before. The effects of changing from DCM to acetonitrile has been studied by Tsierkezos.[49] Tsierkezos has shown that in Fc derivatives the change from DCM to acetonitrile effects both the $E_{1/2}$ as well as the ΔE. The addition of acetonitrile was necessary to solvate the zinc salt, while DCM was needed to solvate $[Dpp\text{-}Fc]_2$. While the complexation of metal ions into a redox active conjugate, such as compound **1**, is expected to result in an anodic shift of the $E_{1/2}$, [50-52] the opposite is observed in this case. Upon addition of Zn^{2+} a further cathodic shift to $E_{1/2}$ = 0.831 V is observed. The rationale provided by others is that the metal ion is able to increase the electron density around ferrocene, therefore allowing for the oxidation of ferrocene to occur at lower potentials which was discussed earlier with regards to figure 3.2b.[48,53] Figure 3.4 shows how the complexation of a zinc ion with **1.**

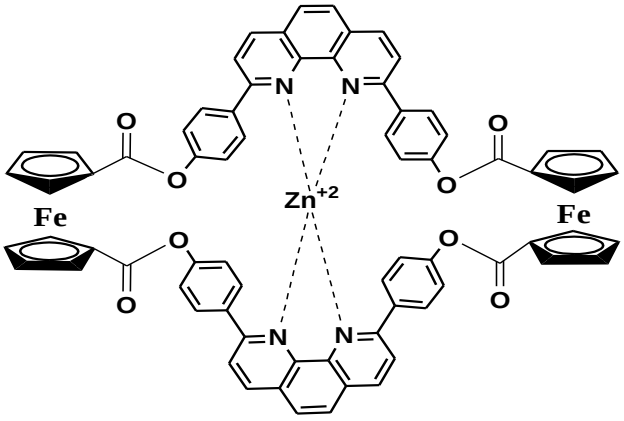

Figure 3.4. Complexation of compound1 with a zinc ion. The complexation may force a change in conformation to align the two phenanthrolines into a bis-bidentating arrangement, which in turn changes the position of the oxygens to the ferrocenes.

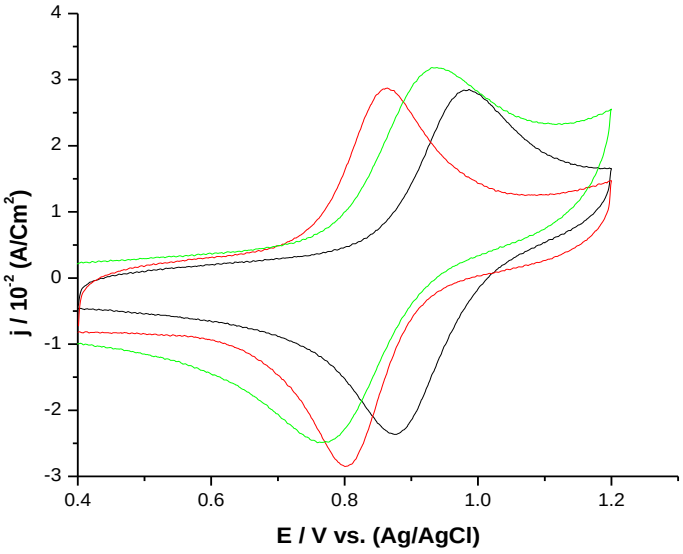

Figure 3.5. CV of **1** at a concentration of 1mM (black) in DCM (Black), in a 2:1 mixture of DCM and ACN (green), in a DCM/ACN (2:1) mixture after addition of Zn^{2+} (red). Scan rate of 500mV/s on a 25μM gold electrode. Potentials are referenced to Ag/AgCl with a Pt counter electrode.

Table 3.1. Electrochemical parameters from CV measurement of conjugate **1** in DCM and DCM/ACN (2:1) in the presence and absence of Zn^{2+}. Error in all measurements is ±5 mV

	i_c/i_a	$E_{1/2}$ (V)	ΔE (V)
1 in DCM	1.22	0.944	0.164
1 in 2:1 DCM:ACN	1.22	0.877	0.159
1 complexed with Zn^{2+} in 2:1 DCM:ACN	1.16	0.831	0.062

.

This complexation might force a conformational change in **1** allowing for electrons to move from the oxygen in the ester onto ferrocene. With the complexation of Zn^{2+} to conjugate **1** there is a large change in the peak separation ΔE, indicating that the redox

event becomes more reversible. Figure 3.6 shows the structure of ferrocenylphthalocyanine, which also displays a significant change in the ΔE as a function of Zn^{2+} coordination to the ligand. In the presence of Zn, the peak separation decreases from ΔE = 226 mV in the absence of Zn^{2+} to ΔE = 93 mV in the presence of Zn^{2+}, indicating a more reversible redox behavior when a zinc ion is complexed.[54] The second set of electrochemical experiment was carried out on the Dpp-AA system. Much like the cyclic $[Dpp\text{-}Fc]_2$ systems there is the potential for metal coordination to the nitrogens of the Dpp group. However unlike the $[Dpp\text{-}Fc]_2$ there is no redox probe in the Dpp-AA systems. This results in the need to use a redox active metal to study the binding of metal ions.

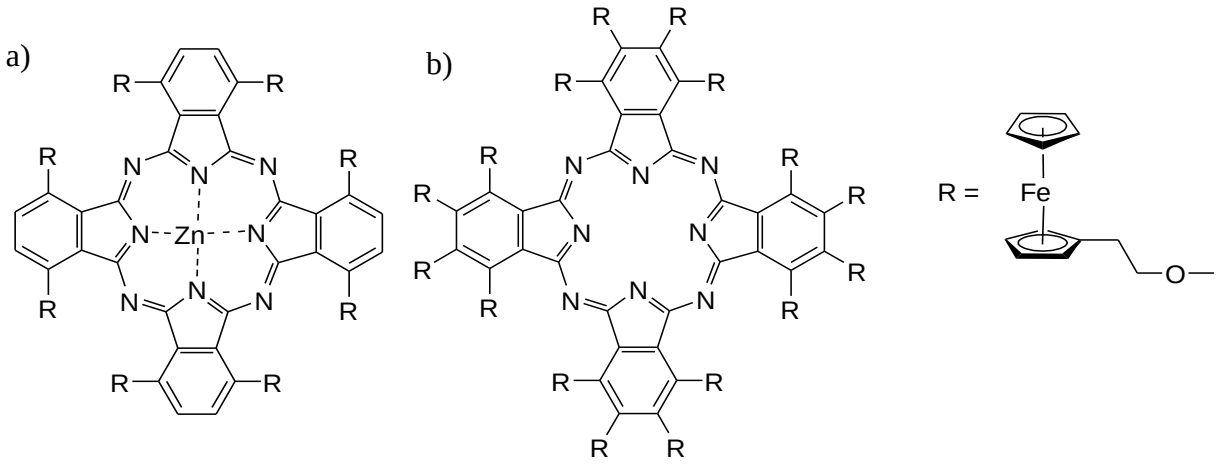

Figure 3.6 a) The separation between the oxidation and reduction peaks in the Zn^{2+}-complex of ferrocenylphthalocyanine is significantly smaller with a ΔE of 93 mV compared to the uncomplexed ferrocenylphthalocyanine (b) which has a ΔE of 226 mV.[54]

Copper was choosen as the redox active metal to monitor the binding in this system. Compounds **2, 4, 6,** and **7**, as well as Dpp itself, were complexed to Cu(I). We chose copper(I) tetrakisacetonitrile hexaflourophosphate as a soluble Cu(I) salt and

explored ligand to metal ratios of 1:1 and 2:1. Then CV studies were carried out on the complexes to see if there was an observable change in the redox potential of the Cu(I). The CV of the Cu(I) complex in ACN is shown in Figure 3.7. It shows a fully reversible one-electron oxidation at $E_{1/2}$ = 0.95 V. Figure 3.8 shows typical CVs of conjugate **2** in the presence of Cu(I) in the ratios of 1:1 and 2:1. As can be clearly seen from Figure 3.8, for a the 2:1 ligand to metal ratio, only one redox active Cu species is present in solution having a $E_{1/2}$ = 0.67 V, while at the 1:1 L:M ratio, two redox signals are observed. One of the redox signals is at the identical position as uncomplexed Cu(I), while the other signal is at the identical position for a CuL_2 complex. This result suggests that after the addition of only one equivalent of ligand, there is still free copper present.

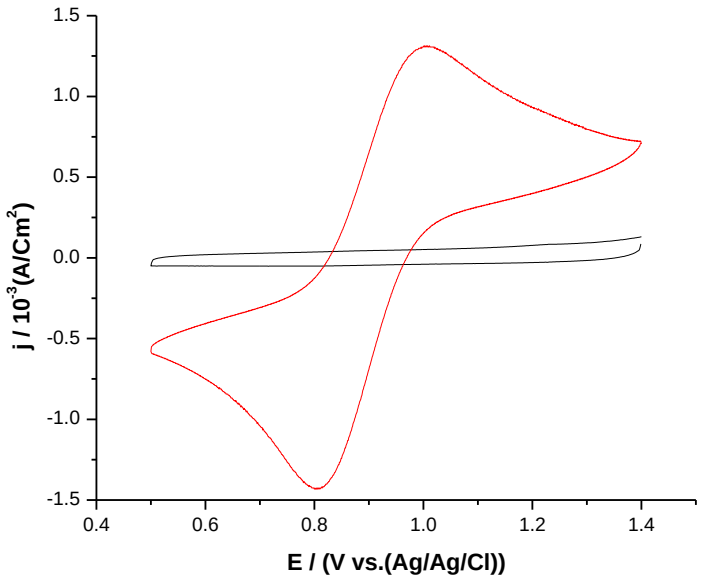

Figure 3.7. Red line, Cyclic voltammetry of $[(CH_3CN)_4Cu]PF_6$; in 0.10 M $LiClO_4$ solution of acetonitrile at room temperature. Black line, background. Working electrode: glassy carbon; scan rate: 100 mV/s.

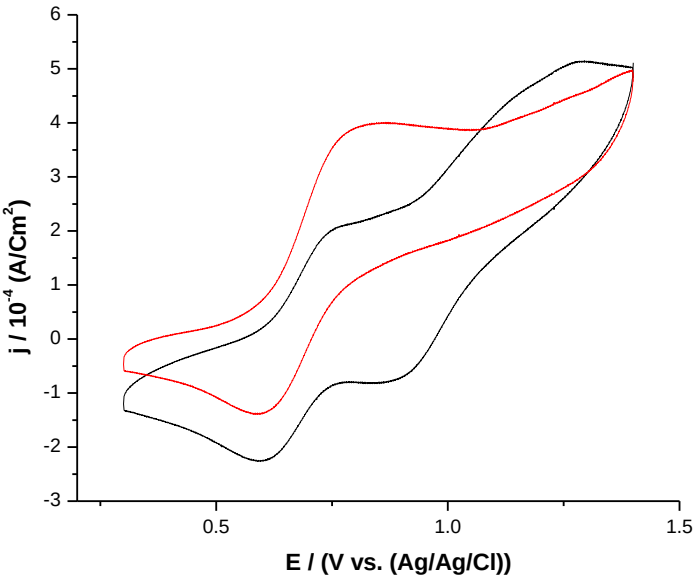

Figure 3.8. Black line, Cyclic voltammetry of $[(CH_3CN)_4Cu]PF_6$ and dpp(-Leu_3-Boc)$_2$ (1:1); red line, $[(CH_3CN)_4Cu]PF_6$ & dpp(-Leu_3-Boc)$_2$ (1:2) in 0.10 M $LiClO_4$ solution of acetonitrile at room temperature. Working electrode: glassy carbon; scan rate: 100 mV/s.

Table 3.2. CV measurements of Dpp, and for the Dpp conjugates **2,4,6** and **7** at 1:1 and 1:2 done in 0.10 M $LiClO_4$ solution of acetonitrile at room temperature. Working electrode: glassy carbon; scan rate: 100 mV/s.

	ΔE (V)		$E_{1/2}$ (V)		i_{pa} / i_{pc}	
$[Cu(CH_3CN)_4]^+$	0.15		0.95		0.98	
Dpp 1:1	0.11	0.50	0.55	0.93	1.23	1.28
Dpp 2:1	0.11		0.54		1.13	
2 1:1	0.07	0.19	0.67	0.90	1.18	0.98
2 2:1	0.10		0.67		0.89	
4 1:1	0.14	0.24	0.67	1.00	0.89	0.90
4 2:1	0.17		0.70		1.26	
6 1:1	0.10	0.17	0.68	0.94	0.90	0.82
6 2:1	0.07		0.68		1.00	
7 1:1	0.10	0.18	0.67	0.94	0.83	0.98
7 2:1	0.10		0.67		1.19	

Table 3.2 summarized the electrochemical properties of Cu(I) complexes in the presence of various M:L stoichiometries. In all cases, the required L:M ratio for the formation of a clean complex was 2:1, indicating the formation of a CuL_2 complex, as would be expected for Cu-Dpp complexes. The fact that when a 1:1 L:M ratio is tested there is free copper and only a 2:1 L:M complex observed and not a 1:1 complex means that phenanthroline has a affinity for 2:1 L:M complexes. This has been seen before in crystal structures where ratios of 1:1 L:M have only grown 2:1 L:M crystals. Figure 3.9 shows an example of a phenanthroline compound that forms 2:1 L:M ratio from 1:1 reactions with cobalt and copper ions.[55] The redox properties of these CuL_2 complexes with L = **2**, **4, 6**, and **7** are essentially identical with $E_{1/2}$ of about 0.67-0.70 V vs Ag/AgCl, indicating that the amino acid and peptide substituents have essentially no influence on the redox properties of the metal center.

2 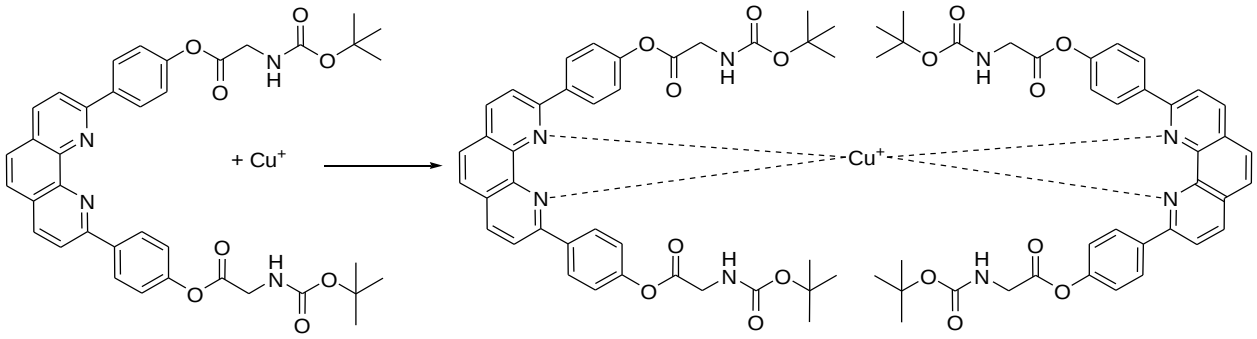

Figure 3.9. Formation of a 2:1 complex obtained even in the presence of equimolar amounts of ligand and metal ion in solution.[55]

As a next logical step, we investigated the metal to ligand stoichiometry of the Dpp-AA-Cu complexes by mass spectrometry. In a typical reaction conjugate **6** was complexed with copper(I) tetrakisacetonitrile hexaflourophosphate in a ratio of 2:1 Dpp-

$(Gly\text{-}Boc)_2$ to Cu. Figure 3.9 depicts a cartoon of how two phenanthroline units can complex a metal letting the amino acid chains move past the other Dpp, which should allow reactions to occur simultaneously on both Dpp-AA compounds. 10 mg of **6** was dissolved in 5 ml DCM followed by addition of 0.5 eq of Cu, this was then allowed to stir for 10 minutes, resulting in the formation of a blood-red solution, which was then examined by mass spectroscopy. Figure 3.11 shows the comparison of calculated and experimental MS, indicating the formation of the expected ML_2 complex.

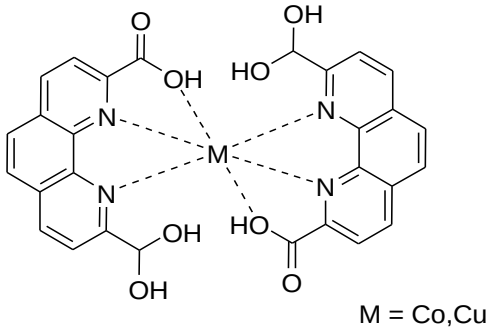

Figure 3.10. Proposed drawing of how two Dpp-$(Gly\text{-}Boc)_2$ units can complex a copper ion.

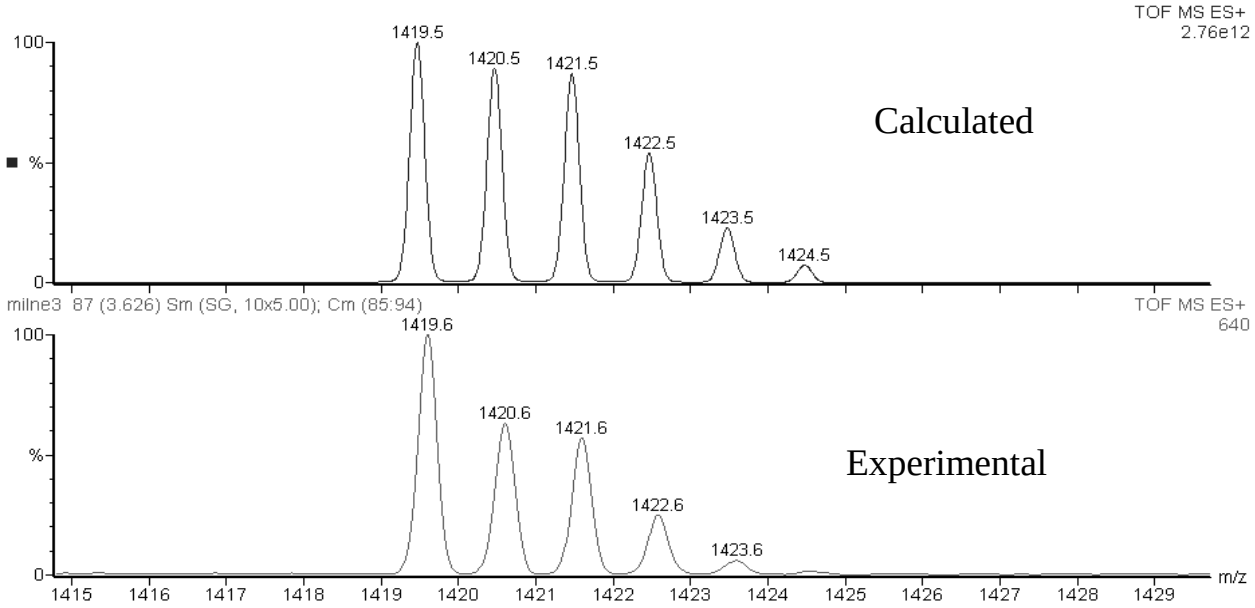

Figure 3.11. MS data for Dpp-(Gly-Boc)$_2$ complexed to a copper ion. Top spectra is calculated, the bottom is the experimental spectra. Isotope patterns for both the calculated and experimental are very close and it is believed that the complex did form

Conclusions

In this chapter, the coordination behavior of Cu^{+} and Zn^{2+} were explored. It was shown by CV and MS studies that the metal ions clearly complex to the Dpp-peptide conjugate presumably by coordinating to the phenanthroline group. In the next section, acyclicpeptide conjugates are explored in an effort to enhance the range of Fc-peptide conjugates that will ultimately be linked to the Dpp ligand.

.

CHAPTER 4.

ACYCLIC FERROCENE PEPTIDE COMPOUNDS

This chapter will focus on the synthesis of additional Fc-peptide scaffolds that are acylic in an effort to enhance the range of molecules that can ultimately be linked to the Dpp group. In particular, the use of diamine linkers will be explored to form bis-Fc conjugates which will have a significantly enhanced ring size.

4.1 RESULTS AND DISCUSSION

In this chapter, the possibility of exploiting the ferrocene (Fc) group as a scaffold to build stable β-sheet mimics will be examined. In particular, the use of diamine peptide spacers that are linked to the Fc group will be used. This was thought to facilitate H-bonding and have enhanced flexibility compared to the related cystamine peptide conjugates. The Fc group is a useful organometallic scaffold for the synthesis of structural mimics for β-sheets and β-turns and metallocene-peptide conjugates have potential applications as potential metallo-drugs[56] and as components in biosensor systems.[57] It has been shown that 1,n'-Fc-peptide conjugates adopt an ordered structure that is stabilized by intramolecular H-bond formation between the proximal amide NH and the carbonyl CO of the adjacent peptide strand as indicated in Figure 4.1. This structural motif was first reported by Herrick and coworkers for $Fc[Ala\text{-}OMe]_2$.[56]

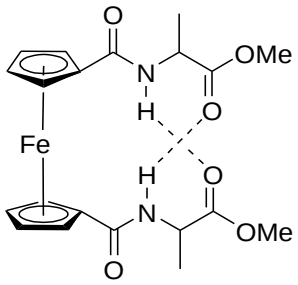

Figure 4.1. Ordered structure observed in compounds of the general formulaFc[CO-AA-OMe]$_{2,}$ as described by Herrick and coworkers. There are two equivalent H-bonds between the proximal amide NH and the distal CO of the adjacent peptide strand, forming a 10-membered H-bond ring.

Similarly, in linear cystamine linked Fc-peptide conjugates, it is the cystamine NH H-bonding with the Fc-CO that "drives" the formation of supramolecular helicates.[58] Cystamine, although flexible, possesses a degree of rigidity due to the conformational preference of the disulfide group. In contrast, an alkyl linker is expected to have enhanced flexibility due to the sp^3-hybridization of the carbon chain. We reasoned that the incorporation of a diaminoalkane linker into an acyclic Fc-peptide framework should enhance the flexibility of the resulting conjugate. In this study Fe[COOH]$_2$ was first coupled to either alanine or glycine, followed by partial hydrolysis and finally attached to an amine linker (Scheme 4.1). 1,4 butyldiamine was chosen as a suitable linker.

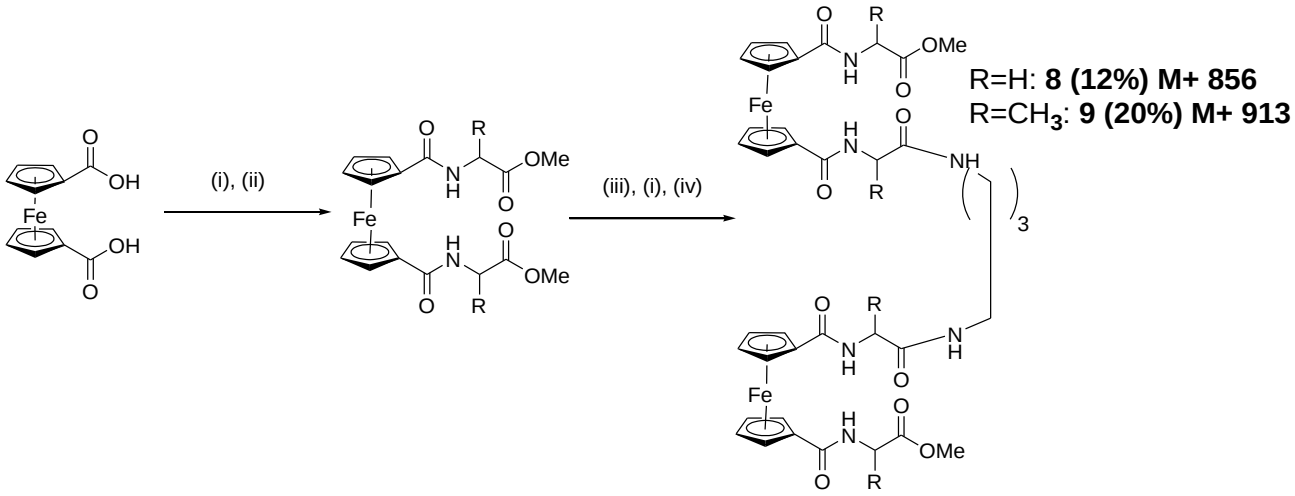

Scheme 4.1. Synthesis of diamine linked ferrocene peptides **8** and **9**. (i) activation by EDC/HOBt in DCM, (ii) Addition of 2.2 eq of H-AA-OMe with 2 eq TEA, (iii) Partial hydrolysis of ester using 1eq NaOH in H_2O:MeOH for 3h. (iv) addition of a solution of 0.4 eq diaminoalkane and triethylamine at 0°C and stirring at room temperature for 20h

It is flexible, which should allow for maximum hydrogen bonding, and in addition has sufficient C-atoms in the chain to allow bending of the conjugate and formation of intramolecular H-bonding interactions. The length of 1,4 butyldiamine is nearly twice the length of a single amino acid. This length choice would hopefully allow the compound to turn back on itself via hydrogen bonds. All compounds were synthesized by amide coupling using EDC/HOBt as shown in Scheme 4.1. Compounds **8** and **9** were obtained as light orange solids in low yields (12-20 %). The lower yields may be due to the presence of inter-strand "Herrick type" H-bonding in the mono acid intermediate which may in fact reduce the reactivity of the carboxy terminus. By using slightly less then 0.5 equivalents of the diamine linker, the purification can be simplified with the only side product being an activated Fc-OBt ester.[59]

In the ^{1}H-NMR spectrum, summarized in Table 4.1, compounds **8** and **9** exhibit the 1:1:1:1 signal pattern typical of disubstituted ferrocenes corresponding to the four

inequivalent Cp protons. The four *ortho* protons with the methyl ester substituent show more downfield chemical shift than those Cp rings with the amide linkage and all *meta* protons are even further upfield in comparison. The α-protons are observed at δ 4.08 and δ 3.86 for **8** and δ = 4.82 and 4.95 for **9**. As is expected for these conjugates, three separate NH resonances are observed ranging from δ 7.95 - 9.23. These relatively downfield chemical shifts compare favourably with those of related cystamine linked symmetrical Fc-peptides and helical Fc-peptide foldamers reported previously that display strong H-bonding interactions.[28,58] Figure 4.2 shows example of ferrocene peptide conjugates that exhibit hydrogen bonding between amides and carbonyls. Comparisons of the amides for Ref 1,2 and 3 to the amide linked Fc peptides are shown in table 4.1.

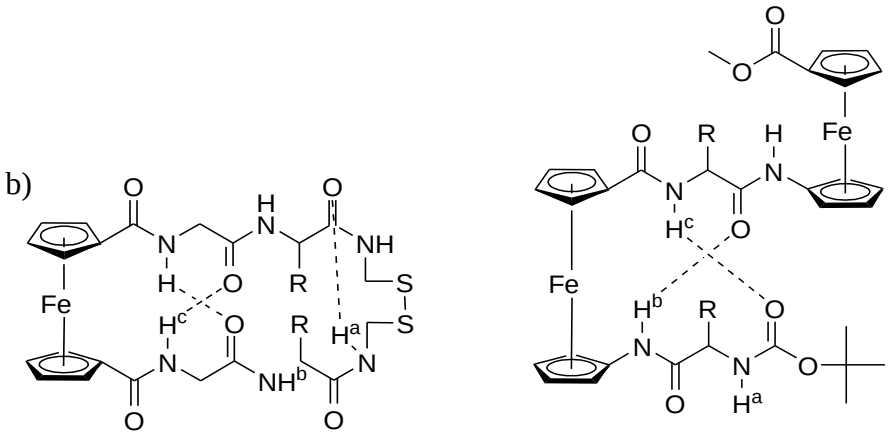

Figure 4.2. a) Drawing of two cyclic ferrocene dipeptide cystamine compounds that show hydrogen bonding which is similar to those seen in compounds **8** and **9**. b) Drawing of a ferrocene peptide conjugate showing intarmolecular hydrogen bonding.

Table 4.1 Selected Spectroscopic data for Fc conjugates **8** and **9** and Ref 1-3 from Figure 4.2

Compound	*^{1}H-NMR* (δ / ppm)			
	NH^a	NH^b	NH^c	αH
8	8.34	9.23	8.26	4.08 3.86
9	8.55	8.97	7.95	4.82 4.95
Ref 1[28]	6.70	7.35	8.31	
Ref 2[28]	6.76	7.18	8.27	
Ref 3[60]	5.28	9.94	8.06	

As can be seen in table 4.1 the only amide that is not hydrogen bonded is H^a for **Ref 3**. The rest of the amides show downfield shifts indicating hydrogen bonding as well as the expected hydrogen bonding in compounds **8** and **9**.

The next step was to study the possibilities of inter and intramolecular hydrogen bonding by NMR studies. A labeling scheme for the amide protons is provided in Figure 4.3a. A concentration dependent ^{1}H-NMR study was first performed on compounds **8,9** and showed no effects on the amides (Figure 4.3b). This is indicating that none of the amides are participating in intermolecular hydrogen bonding.

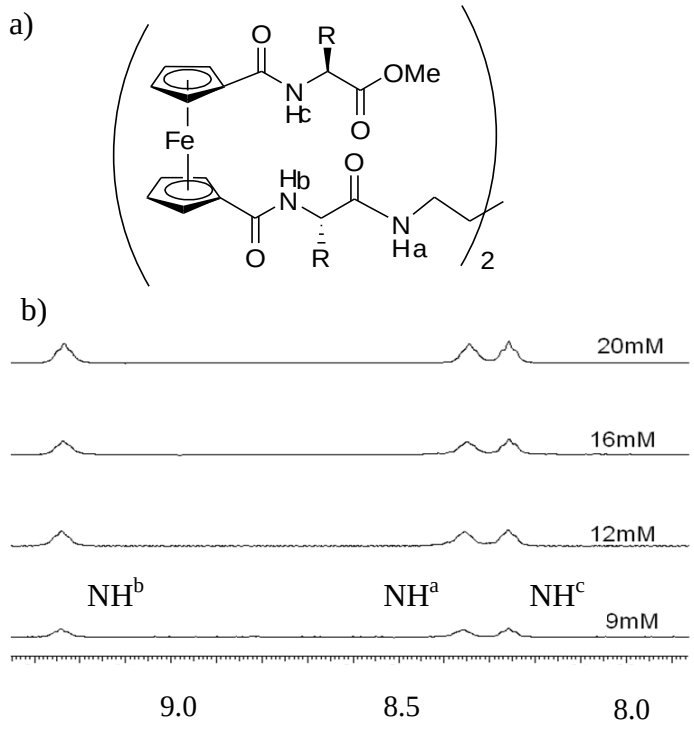

Figure 4.3. a) Labeling scheme for compounds 8 and 9. b) Concentration dependent NMR for 8 showing amides. No shifts are present, indicating there is no intermolecular hydrogen bonding present.

VT-NMR studies were then carried out in $CDCl_3$ solution on compounds **8** and **9** to further investigate the H-bonding behavior of these Fc-conjugates. All three amides display temperature dependent chemical shifts as shown in the ^{1}H-NMR spectra amide region (Figure 4.4a). This indicates all three amides involvement in H-bonding, and temperature behavior is outlined in Figure 4.4b.

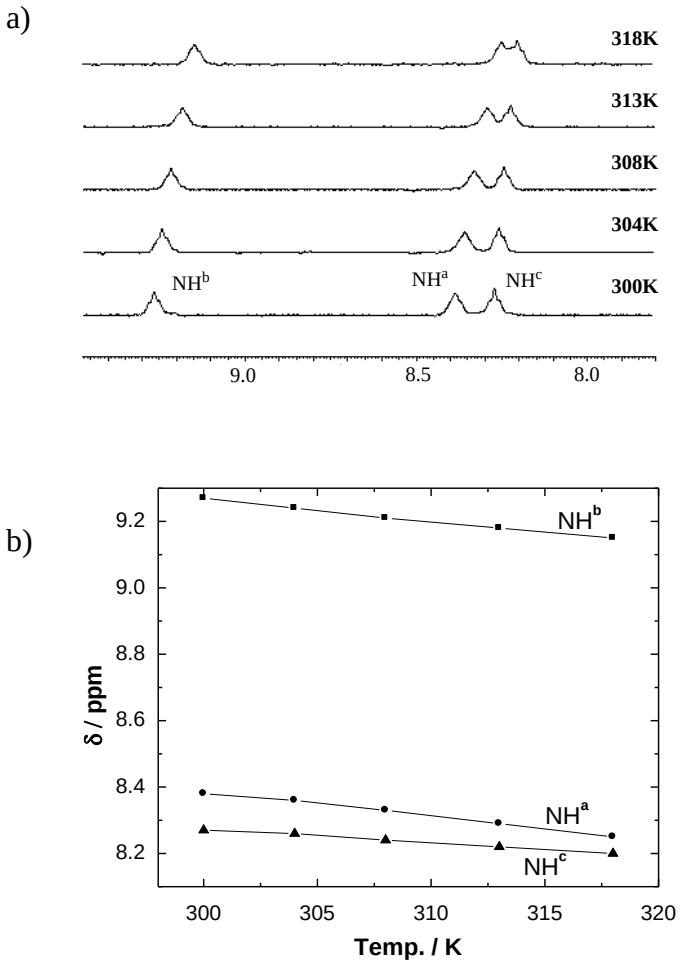

Figure 4.4. a) Variable temperature ^{1}H-NMR spectra of compound **8** showing the amide NH region only. Shifting of all three amides to lower ppm indicates that intramolecular hydrogen bonding is present. b) Plot of the δ of the amide NH vs. the temperature in °C.

The temperature coefficients clearly indicate the involvement of NH^b and NH^a in H-bonding (for compound **8**: NH^a = -7.4 ppb K^{-1}; NH^b = -6.6 ppb K^{-1}; NH^c = -4.0 ppb K^{-1}, compound **9**: NH^a = -6.2 ppb K^{-1}; NH^b = -5.5 ppb K^{-1}; NH^c = -3.5 ppb K^{-1}). The temperature coefficients for the Fc-proximal amide NH^c is significantly lower, indicating potentially weaker H-bonding. The temperature dependences are similar to other Fc-peptide systems able to engage in H-bonding interactions.[61]

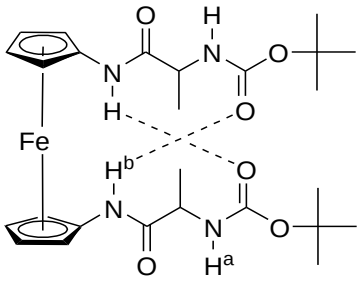

Figure 4.5. Drawing of a ferrocene peptide having intramolecular hydrogen bonding that was studied by variable temperature ^{1}H NMR.[61]

The temperature coefficients for the compound in figure 4.5 are NH^{a} = +4.2 ppb $K^{-1}$and NH^{b} -6.9 ppb K^{-1}. These results are indicating that the amide closest to Fc is hydrogen bonded intramolecularly and the value of -6.9 ppb K^{-1} for the temperature coefficient is similar for results shown for compound **8** and **9**.

The diamine linker amide NH displays the most pronounced dependency of temperature on the chemical shift, indicating stronger H-bonding than for the amino acid amide NHs. For the intramolecular H-bonding to occur without any intermolecular H-bonding one can assume that the introduction of the diamine linker has introduced sufficient flexibility into the system to allow formation of the "Herrick H-bonding pattern" which enables also the participation of the diamine NHs as proposed in Figure 4.6. By continuing in this fashion a long ferrocene peptide diamine system could result in a fairly good representation of a β-sheet in solution.

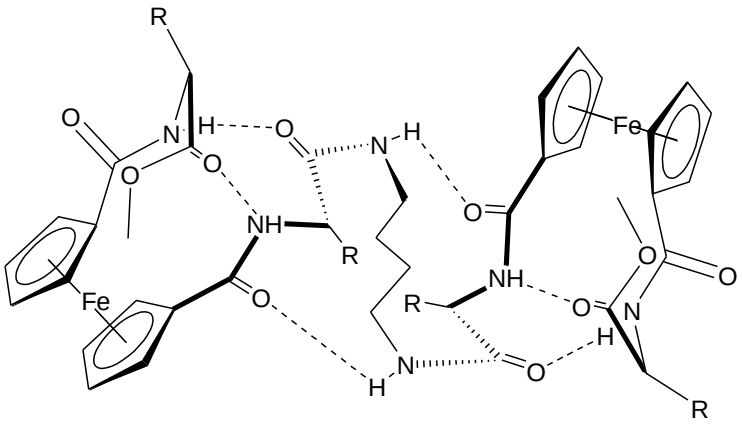

Figure 4.6. Proposed solution structure of compounds **6** and **7** based on VT-NMR studies showing that all amides are present in intramolecular hydrogen bonding. Drawing illustrates the proposed folding of the compound with ferrocene as a turn inducing element. Dashed lines indicate proposed hydrogen bonding interactions.

Next, the electrochemistry of compounds **8** and **9** was studied by cyclic voltammetry (CV) in a DCM solution. During a cyclic voltammetry experiment the ferrocene becomes oxidized from an iron 2^+ species to an iron 3^+ and back again during the reverse reduction scan. As the oxidation occurs in a system where there are two or more redox centers there is the possibility of two different electrochemical scenarios occurring. The first is when the two redox centers act independently of each other and only one oxidation peak is observed. This occurs when there is no electronic communication between redox centers and therefore the two ferrocenes will be oxidized and reduced at the same potential compared to each other. The second scenario is when the two redox centers are affected by each other. This effect causes one of the potentials to shift to higher potentials indicating that the ferrocenes can sense each other, resulting in oxidation of one of the ferrocenes being at higher potentials or more difficult to oxidize. This occurs because of the electronic communication between the ferrocenes. As one ferrocene becomes 3^+, it inherently makes the oxidation of the other ferrocene more

difficult. Figure 4.7 has examples of systems containing two ferrocenes that show electronic communication between ferrocene groups, resulting in two oxidation peaks during CV experiments.

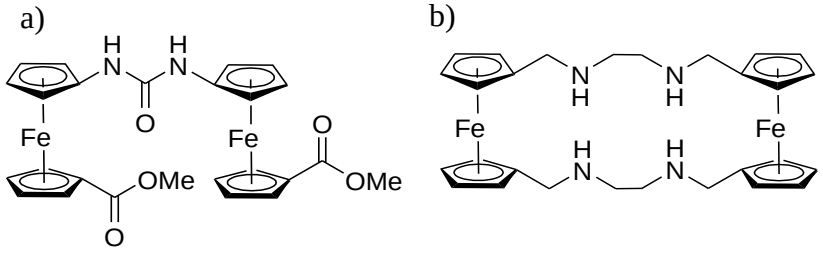

Figure 4.7. a) Two ferrocene system that exhibits oxidation of ferrocene at 422 mV and a second peak at 559 mV.[61] b) A two ferrocene system in which both ferrocenes show no electronic communication to one another resulting in simultaneous oxidation at 20 mV.[62]

The difference in the two examples shown in figure 4.6 is conjugation between the two ferrocene moieties. It has been shown as the conjugation between the ferrocene centers increases so does the communication. This effect has led research into molecular wires using conjugated ferrocene systems.[63]

With two ferrocene units in both **8** and **9** there is the possibility to have electronic communication between the two redox probes but this is not expected because the two ferrocene groups are linked by an alkyl chain and conjugation between the ferrocene groups is not present. As a result of no conjugation both systems display a single reversible one electron oxidation. Both ferrocenes are oxidized and reduced at the same redox potential (Figure 4.8). A variable scan rate experiment was carried out in which the CV was recorded at various scan rates. Figure 4.8 shows a linear dependence of the square-root of the scan rate with the peak current for compound **8** and **9** as would be

expected for redox species in solution (Figure 4.9) Table 4.2 summarizes the electrochemical results.

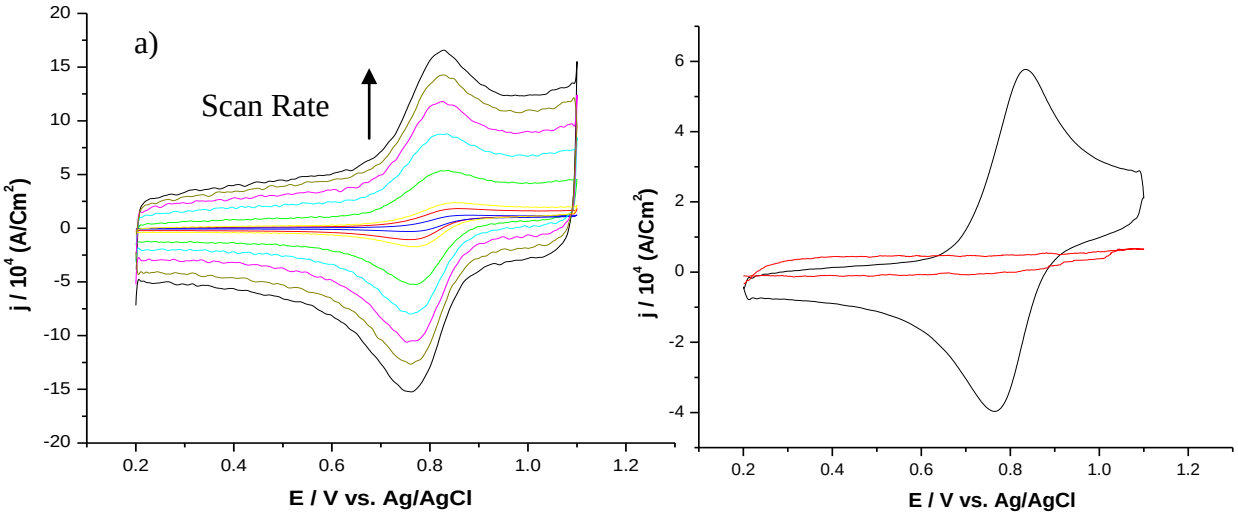

Figure 4.8. CV of compound **8** with background in red, at a concentration of0.3 mM with 1.0 M TBAP as the supporting electrolyte. Scan rate of 1.00 V/s on a 25 µM gold electrode in DCM. Potentials are referenced to Ag/AgCl with a Pt counter electrode. $E_{1/2}$ = 0.80 V, i_a/i_c = 0.77. ΔE = 0.07V

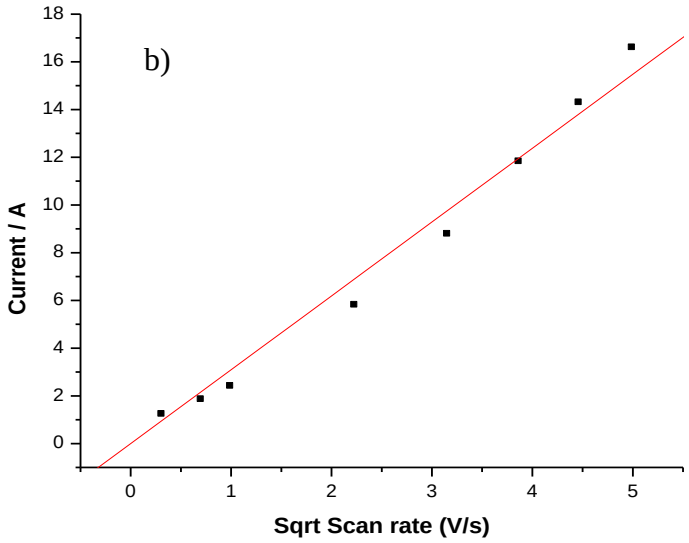

Figure 4.9.a) CV of compound **9** at a concentration of 0.3 mM with 1.00 M TBAP as the supporting electrolyte. Scan rate of ranging from 0.10 V/s to 25 V/s on a 25 µM gold electrode in DCM. Potentials are referencedto Ag/AgCl with a Pt counter electrode. b) Graph of relationship of current vs. √scan rate for compound **9.** The linear relationship indicates that the system is diffusion controlled

Table 4.2. CV measurements of compounds **8** and **9** at a concentration of 0.3 mM with a scan rate of 1 V/s on a 25 μM gold electrode in DCM . Potentials are referenced to Ag/AgCl with a Pt counter electrode.

Compound	ΔE (mV)	$E_{1/2}$ (mV)	i_a/i_c
8	71	799	.77
9	84	812	.88

It has been shown that ferrocene can be used as a scaffold for beta sheet mimics. By selecting a linker of the correct length, flexibility, and hydrogen bonding possibilities, it is possible to build ferrocene peptides that are only intramolecularly hydrogen bonded. Having only intramolecular hydrogen bonded beta sheets gives the advantage of doing electrochemical studies at any concentration and without having to worry about the effects of intermolecular hydrogen bonding. It should be noted that compounds **8** and **9** can be lengthened by the process of hydrolysis followed by peptide coupling to create a larger beta sheet mimic.

Conclusion

In this chapter, a series of diamine-linked ferrocene peptides were prepared. These molecules display strong intramolecular H-bonding interactions, presumably leading to the formation of sheet-like arrangements in solution and the solid state. Additional studies will need to be carried out in the future in an effort to investigate the structural properties in more detail.

CHAPTER 5.

TOPOLOGICALLY LINKED MOLECULES

Topologically linked molecules are two or more molecules that cannot be separated without breaking a covalent bond. This category of molecules includes catenanes and rotaxanes, where cantenanes possess two or more cyclic molecules physically connected through space but not covalently bonded to each other. Rotaxanes are similar to catenanes in that there is a cyclic component but in a rotaxane there is also a linear component which passes through the cyclic molecule. This chapter describes the synthetic attempts to develop new topologically linked Fc-peptide conjugates based on marcocycles developed earlier.

5.1 NATURALLY OCCURRING TOPOLOGICALLY LINKED PROTEINS

In recent years there has been the discovery of topologically linked proteins. There has always been the prediction that proteins could possibly be mechanically linked, but not until the last ten years has there been proof. In 2000 Wilkoff and co workers solved the highly complex crystal structure of the bacteriophage HK97.[65] The outer protein shell (capsid) of the virus was shown to have 72 interlocking rings with each ring being topogically linked to either five or six other rings, giving rise to a “chainmail” structure (Figure 5.1).

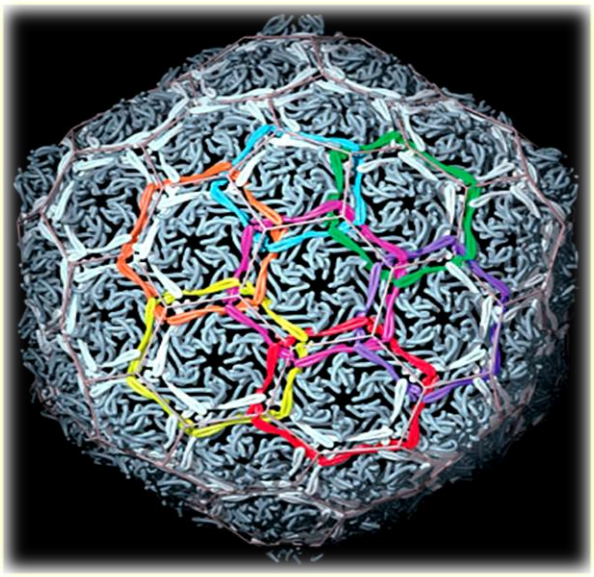

Figure 5.1. Crystal structure representation of bacteriophage HK97. Each colour represents one of the 72 subunits which are interlocked to neighboring subunits, giving rise to a capsid consisting of fully interlocking proteins.[65]

Research has shown that interlocking proteins have an increase in thermal stabilization as well as a higher stability to chemical denaturation.[66,67] These types of discoveries have lead researchers to synthesize their own topologically linked peptides to better understand the synthetic pathways and folding nature uses to develop rather complicated system.[68,69]

5.2 MOLECULAR MACHINES

As technology increases so does the demand for the miniaturization of electronics. The goal of creating the smallest, lightest, and most convenient product has lead research to examine the use of molecular machines to aid in this goal. Topologically linked

molecules have been thought to be able to act as molecular machines because of their ability to move a single component of the molecule while keeping another part stationary, resulting in molecular movement. When thinking of rotaxanes it is easy to see how if the cyclic component moved independently of the linear portion, it could be used as a shuttle. The shuttle idea has lead research to use molecular rotaxanes in drug delivery systems,[70] memory storage devices,[71] and to act as switches for electronics.[72] Figure 5.2 shows a rotaxane that is used as a memory storage device similar to a computer's hard drive. It is believed that because of the size of a single molecule it is possible to reach higher density packed memory devices using similar molecules.

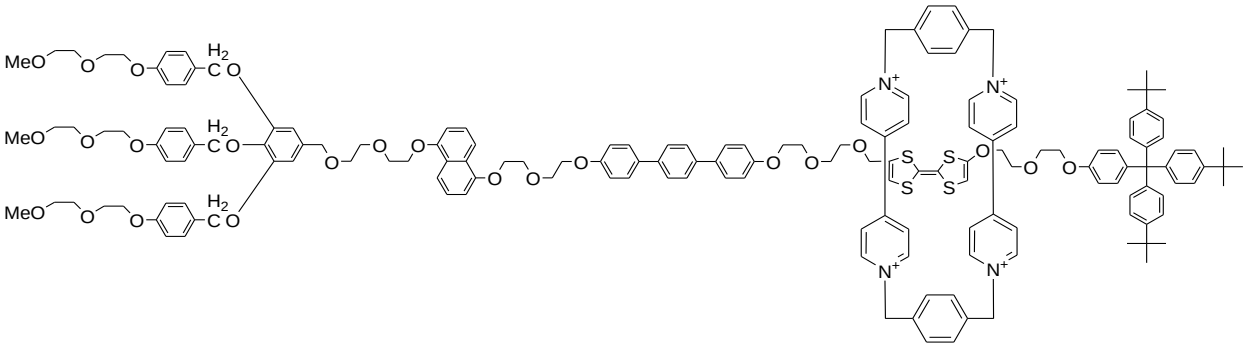

Figure 5.2. Structure of a rotaxane that is currently being tested for its possibility to develop a high density packed memory device. This particular rotaxane possesses two positions for the cyclic component to reside, thus being a potential binary storage device.[71]

5.3 SYNTHESIS

The synthesis of topologically linked molecules can be carried out in a number of ways and will be described briefly. In any cyclization reaction there is the chance that catenanes will be produced, but this percent is very low and is not used. Here I will introduce two variations of the templating technique. In the first approach, two independent molecules are coordinated to a metal ion, allowing their reactive groups to

cross each other, followed by the cyclization of both molecules. The second technique is synthesis a cyclic compound which then can be templated to an acylic compound, followed by cyclization of the acyclic compounds around the starting cyclic compound. Figure 5.3 shows how both techniques can be used when templated with a metal. Templating can also be used for rotaxane synthesis, if the linear component of the rotaxane has a metal coordinating site.

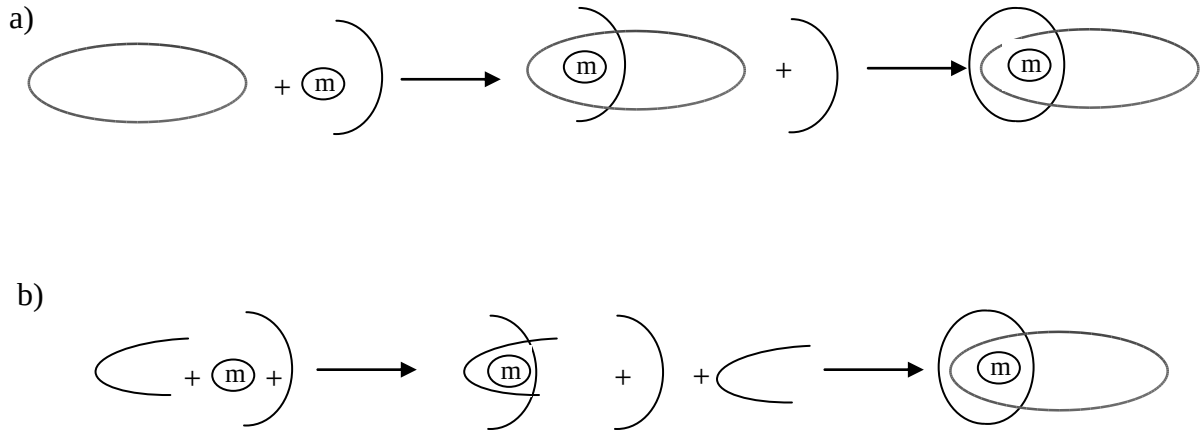

Figure 5.3. Two synthetic techniques described by Sauvage *et al*. a) For catenane synthesis, the first step is to template the macrocycle with a metal, followed by allowing the acyclic component cross past the macrocycle, followed by cyclization of the second ring, forming a catenane. b) Two acyclic components are templated to a metal center, followed by cyclization of both acyclic components.[29,62]

While metal templating can work for systems where there is a metal chelation site, some systems do not contain such a site and need different stabilizing effects. Vögtle and co-workers have shown how H-bonding involving amides NHs can be used to stabilize intermediate systems which can then be reacted to form topologically linked systems.[73] In the synthesis of these amide template systems, the first step is to synthesis a macrocycle that contains amide bonds, followed by inserting a guest molecule that can be held in the center of the cyclic component through hydrogen bonds. This is then followed by either capping the guest molecule resulting in the formation of a rotaxane or its cyclization it into a catenane.

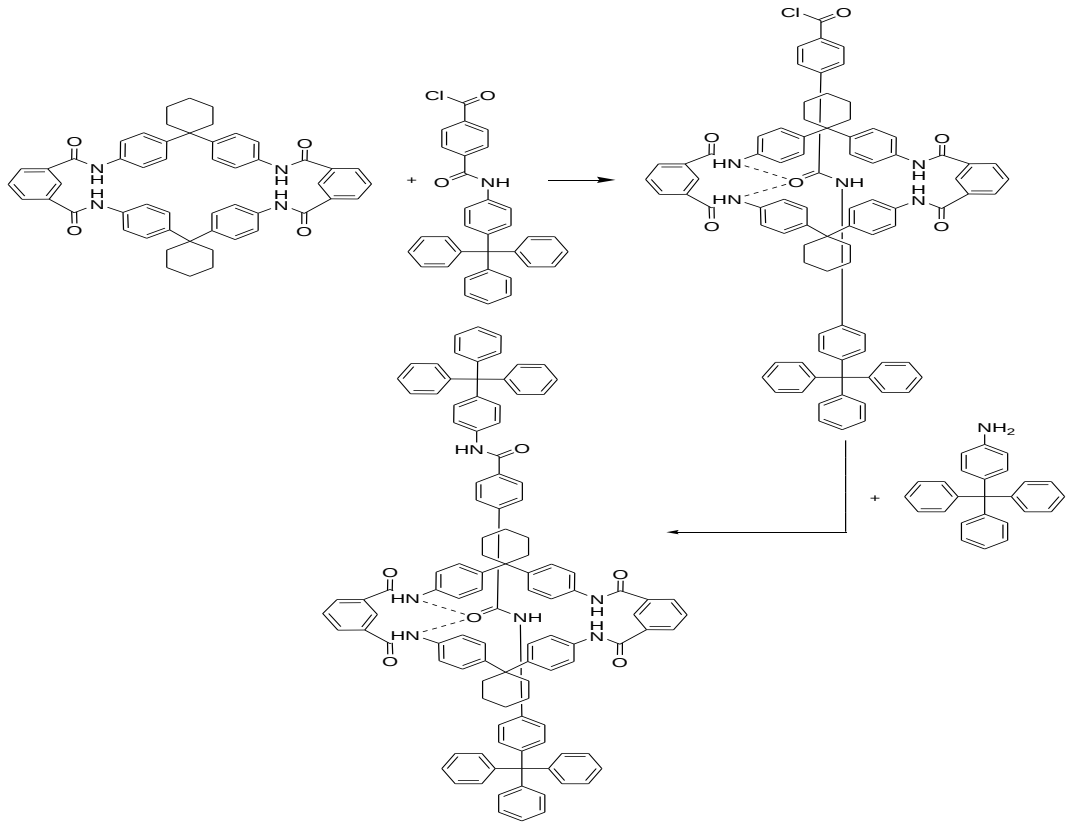

Figure 5.4 Possible intermediate in the synthesis of an amide templated rotaxane. For synthesis of rotaxanes it is important that the capped sting does not slide through the cyclic molecule once synthesis is complete. Selection of a large capping agent like trityl phenol is used to prevent the sliding of the ring off of the linear molecule.[73]

Figure 5.4 summarizes the synthesis of a rotaxane by involving the formation of H-bonding between the cyclic component and the linear component, followed by capping with bulky groups. This will prevent loss of the host.[73]

5.4 EXPERIMENTAL ATTEMPTS TO ROTAXANES AND CATENANES

As can be seen by research by Sauvage[62] and Vögtle[73], it should be possible to synthesize topologically linked peptide conjugates making use of compounds **2**, **4**, **6**, and **7**. Results described in Chapter 3 indicate that when compounds **2**, **4**, **6** and **7** are coordinated to a Cu(I) centre, the Boc protected amide ends will be crossing each other allowing for cyclization around each other as indicated in Figure 5.3, and thus catenation reactions should be possible. This type of reaction was attempted many times without any conclusive results.

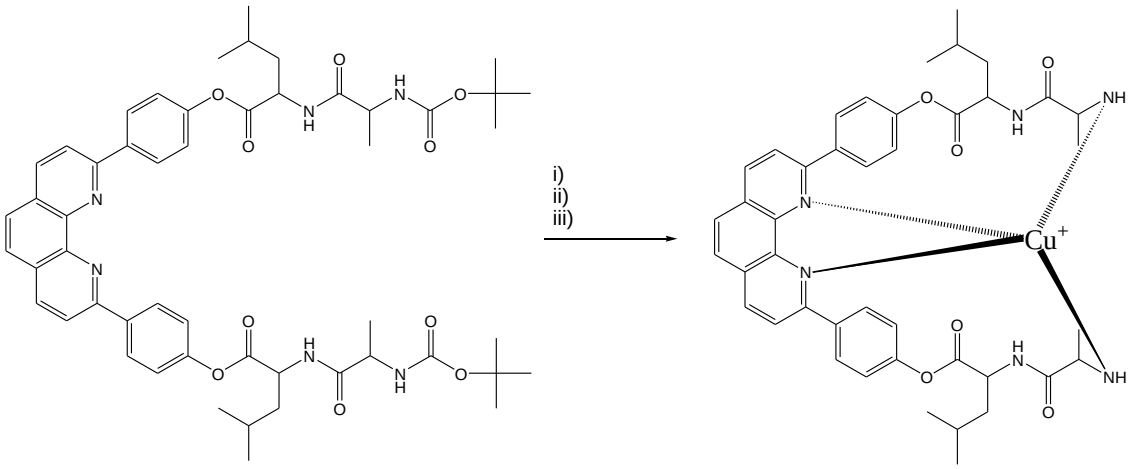

Scheme 5.1 Attempted catenane reaction using Dpp-(Leu-Ala-Boc)$_2$. i) Addition of $[Cu(MeCN)_4]BF_4$ ii) Boc removal by addition of 1 mL TFA in 1mL DCM. iii) Slow addition of $Fc[COCl]_2$. Final compound precipitated out of DCM and it was not able to be used towards catenane reaction.

The major difficulty arising during the catenation of Dpp-$(AA\text{-}Boc)_2$ appears the affinity of the N-terminal amino group for the Cu(I) center. Scheme 5.1 shows an attempted catenane reaction using compound **7** and the predicted final product**.** It is believed that upon removal of the Boc group, the N-terminal amino group will complex to the Cu(I), which essentially decreases its nucleophilicity to such an extent that it is unavailable for the reaction with $Fc[CO\text{-}Cl]_2$. Mass spectrometry experiments were carried out on this compound and the results indicate that a copper complex was formed with a single Dpp-LA compound. The Boc-group was clearly absent. The complex exhibits the appropriate isotope pattern for a copper complex (Scheme 5.1). Other attempts, such as adding the Cu(I) after Boc deprotection, did not alter the results and essentially the same complex was obtained.

Similar complexation patterns have been described before in the literature and are directly relevant to the results of the MS study and shed light on a potential coordination environment of the Cu(I) centre in our Dpp complexes. Studies to determine the affinity of amino acids to transition metals to help understand the biological function of metals have been performed before and have shown similar binding to the predicted system for the [CuDpp-LA] complex.[74-76] Figure 5.5a shows the binding pattern for [Cu(1,3,5-triaminocyclohexane)(Gly)]$^+$ with the corresponding crystal structure in Figure 5.5b.[75] In this system the glycine complexes the Cu ion through the terminal amino group as well as the oxygen of the C terminus. Figure 5.5c shows a drawing of $Cu[Aib_3]$. The coordination environment of the Cu ion includes two backbone amides and the N-

terminal amino group along with the oxygen of the C terminus in a square planar geometry. The corresponding crystal structure is shown in Figure 5.5d.[76] It should be noted that when these amino acids are complexed to copper the pKa of the amine and the backbone amide NH is reduced significantly.

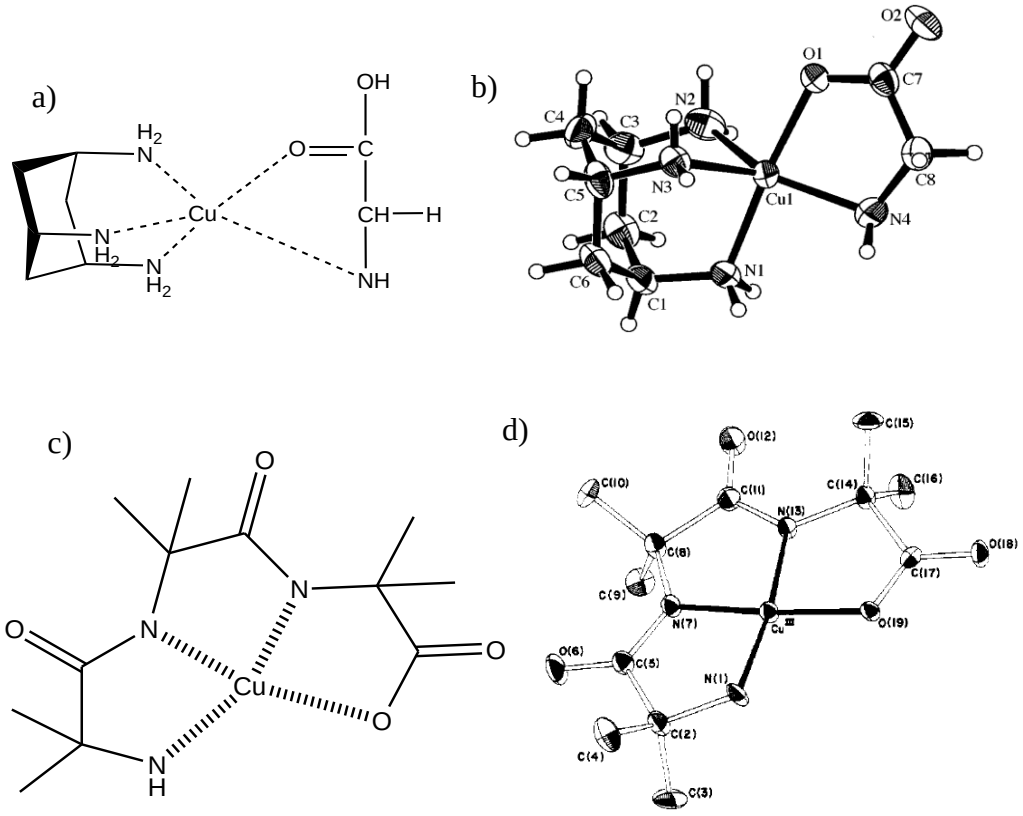

Figure 5.5 a) Drawing of the binding structure for Cu(1,3,5-triaminocyclohexane)(Gly)]$^{+}$. b) ORTEP plot of Cu(1,3,5-triaminocyclohexane)(Gly)]$^{+}$ with the deprotanted amine and the carbonyl of glycine complexed to Cu^{+}.[75] c) Drawing of Cu(III)Aib$_3$ showing squar planar geometry with three N and one O coordinating to the Cu cation. d) ORTEP plot of Cu(III)Aib$_3$.[76]

Scheme 5.2 shows another attempt at a topologically linked system making use of cyclo-Fc[CO-Leu]2-1,4butyl diamine. In this synthesis, this Fc-peptide conjugate was

used as a precursor for rotaxane synthesis based on Vögtle's amide hydrogen bond synthesis.

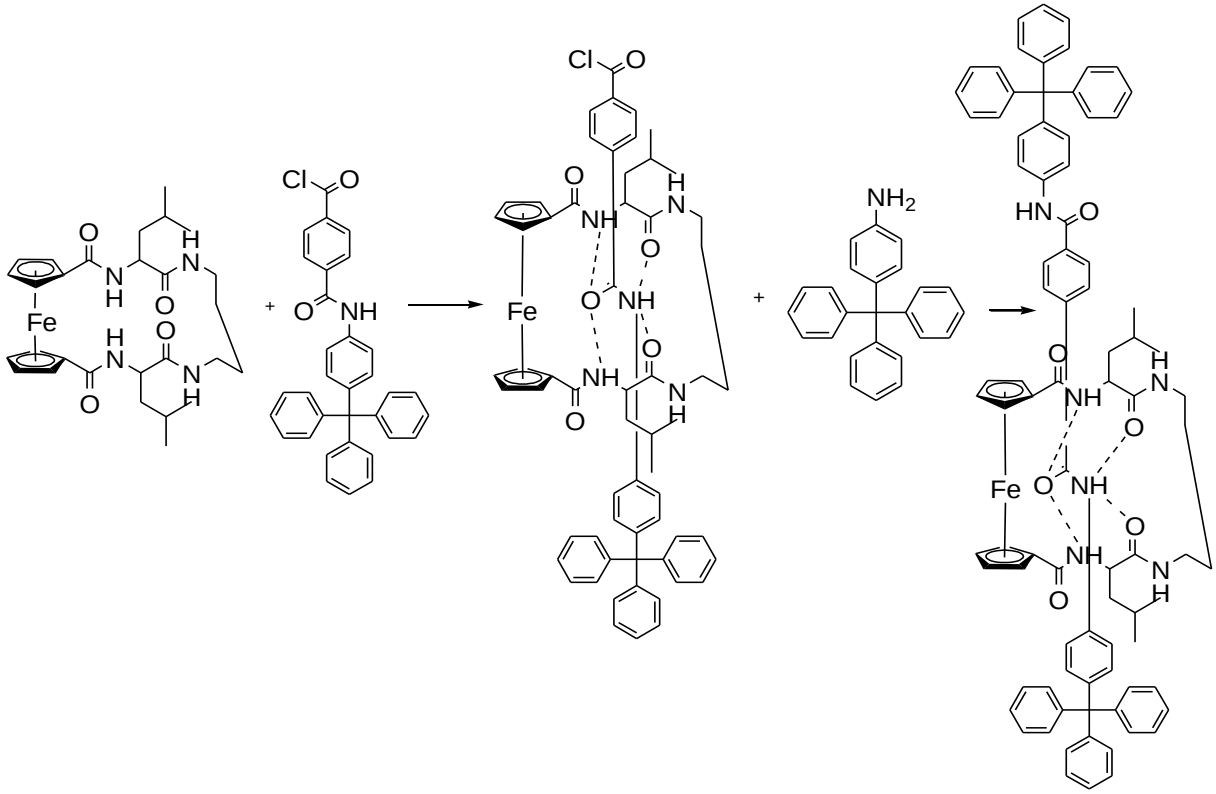

Scheme 5.2. Attempted rotaxane synthesis using cyclic Fc[CO-Leu]$_2$-1,4 butyl diamine as the cyclic component followed addition of a linear component with the potential to hydrogen bond the amides of leucine followed by the addition of a capping trityl group.

During the attempted synthesis of the rotaxane shown in Scheme 5.2, TLCs were employed to monitor the reaction. At the start of the reaction a single yellow spot was observed, after addition of the linear component two yellow spots were observed, one with the same R_f as the starting material and a new compound. After the addition of the trityl capping group and work up the crude mixture was purified by column chromatography, resulting in the isolation of only the starting ferrocene material with nearly 99% recovery. Because of these results it is believed that the linear component

may be interacting with the cyclic ferrocene compound through hydrogen bonding but the interaction may not be desired interaction leading to the formation of the rotaxane. A possible explanation is that there is an interaction of the "linear component" with the outside amides of the cyclic component or that a potential rotaxane is formed but is unstable under the isolation conditions. As column chromatography is performed the two components are separated resulting in nearly full recovery of the starting cyclic ferrocene component. Although, unsuccessful in the attempts described here, the possibility to synthesize topologically linked peptides should be possible. Clearly additional work is necessary on finding conditions suitable to carry out the ring closure. MS experiments clearly show that a Cu-complex is formed. However, it appears that the nucleophilicity of the Cu-coordinated amine is too low to ensure reaction even with acid chlorides. It will be necessary to investigate this aspect in more detail before a successful peptide rotaxane or catenane can be obtained.

Conclusions

In this chapter describes our attempts to prepare Fc-peptide-Dpp catenanes and rotaxanes. While it appears that the preparation of such systems was unsuccessful, their preparation remains a useful goal that should be attempted in the future.

CHAPTER 6.

GENERAL DISCUSSION AND CONCLUSIONS

In this thesis it has shown that a number of new cyclic and acyclic ferrocene peptide conjugates have been synthesized and characterized. By combining ferrocene peptides with diphenol phenanthroline it has been possible to synthesize a number of cyclic compounds that exhibit both redox properties as well as metal complexing while still contributing to cyclic peptide models. By comparing the crystal structures compound **1** which contains no peptides $[DppFc]_2$ to compound **3** that contains four lecucine residues $Dpp(Leu_2)_2$-Fc it is evident that hydrogen bonding directs the crystal packing of these systems while π stacking is secondary and only seen in compound **1** when there is no possible hydrogen bonding interactions. The redox property as well as the metal binding ability of compound 1 was also studied. By performing cyclic voltammetry experiments on compound **1** it was observed that cationic metal binding shows an unusual cathodic shift of roughly 40mV, which has been explained as a conformational change resulting in an increase of electron density around ferrocene. Compounds **2,4,6** and **7** were also studied electrochemically for their binding ability to copper. In this study different ratios of the L:M were studied by cyclic voltammetry. The ratios of 2:1 and 1:1 were tested to observe how the copper was being complexed. It was evident from the electrochemistry that Dpp compounds have a high tendency to form

dicomplexed species even when a ratio of 1:1 L:M is used. This result was then backed up by literature where only dicomplexed Dpp systems have been crystallized even when a 1:1 L:M ratio was used, as well as the mass spectrometry results that always show a dicomplexed species present.

Future research recommendations in this area can be seen in the development of monitoring of ions. The Dpp unit of these compounds allow for a size constrained complexation site while ferrocene has been shown to be affected by the complexation of metals. If a change in size effects the conformational change of the system then it should be possible to monitor different metals based on their size and perhaps their charge. A second future research area was discussed earlier in chapter 5. Topologically linked molecules can be synthesized from the cyclic compounds **3** and **5.** This research area however can be seen as fairly complicated both because of the low yields of cyclization as well as the reactivity of amides to the metals that are needed in catenation reactions.

In a second study of ferrocene peptide synthesis a β-sheet model was made by combining butyl diamine with either two Fc-1-(gly-OMe)-1`-(gly-OH) or two Fc-1-(ala-OMe)-1`-(ala-OH). In doing this it was possible to develop a completely intramolecular hydrogen bonded system that is completely independent to concentration while being dependent on temperature. For this to be useful suitable peptides could be chosen that allows for salvation of a ferrocene peptide system in water, followed by electrochemistry of potential beta breakers could be examined to screen or predict disruptions of the intramolecular hydrogen bonding.

CHAPTER 7.

EXPERIMENTAL

6.1 GENERAL PROCEDURE

All experiments were performed using CH_2Cl_2 that was distilled and dried (CaH_2) prior to use. The coupling agents used for amide bond formation, *N*-ethyl-*N′*-(3-dimethylaminopropyl) carbodiimide hydrochloride (EDC·HCl) and 1-hydroxybenzotriazole hydrate (HOBt) (Advanced ChemTech) were used as received. H-Leu-OMe·HCl, triethylamine, sodium hydroxide (Sigma Aldrich) were also used as received. Ferrocene dicarboxylic acid ($Fc[COOH]_2$) was synthesized as described previously.[77] Ferrocene diacid chloride ($Fc[COOCl]_2$) was synthesis as described previously 78. Dpp was synthesized according to reference 79. All reactions were carried out in air unless specified. For column chromatography a column was packed 15-25 cm high with 230-400 mesh silica gel (Silicycle). Nuclear Magnetic Resonance (NMR) spectra were recorded on a Varian Mercury 400 spectrometer operating at 400.1 MHz for ^{1}H-NMR and 100.6 MHz for ^{13}C-NMR. Both ^{1}H-NMR and ^{13}C-NMR were reported in ppm relative to tetramethylsilane (TMS, $\delta = 0$). The ^{1}H-NMR spectra were referenced to the residual signals of $CHCl_3$ (δ 7.26) or CH_3OH (δ 3.31). All ^{13}C-NMR were referenced to the $CDCl_3$ signal (δ 77.23) or CH_3OH (δ 49.00). 2D-COSY experiments were used to complete assignments in the ^{1}H-NMR spectra. Mass spectrometry analysis was carried out using a Finnigan MAT 8200 (Doug Hairsine of the University of Western Ontario Chemistry Department). Infrared spectra were obtained on a Bruker Tensor 27 FTIR spectrometer. Cyclic voltammetry experiments were performed using a CHI900b instrument at room temperature (22 ± 2 °C). A working microelectrode of carbon was used against an Ag/AgCl reference electrode and platinum counter-electrode. All

samples were prepared as 0.5 mM solutions in distilled dichloromethane with 0.2 M tetrabutylammonium perchlorate (TBAP) as a supporting electrolyte. The scan rate was varied from 100 – 2500 mV s^{-1} for all compounds.

Preparation of $[FcDpp]_2$ (1)

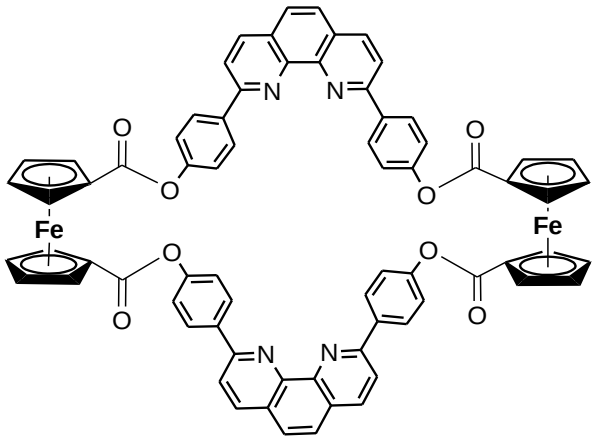

A solution of ferrocene diacid chloride 310 mg (1 mmol) and 366 mg (1 mmol) Dpp was stirred in 200 mL DCM. This solution was then refluxed for 10h, followed by an aqueous workup, involving consecutive washings with saturated $NaHCO_3$, 10% citric acid, and finally distilled water. The organic phase was collected, dried of Na_2SO_4, filtered and evaporated to dryness. The crude product was then purified by column chromatography with a mobile phase of 1% TEA in EtOAc. The final product is only soluble in chlorinated solvents and has shown some impurities in NMR. (R_f = 0.20) (55 mg, 5%).

^{1}H NMR ($CDCl_3$, δ in ppm): 8.40 (8 H , d, Dpp) ; 8.05 (4 H, d, Dpp) ; 7.92 (4 H, d, Dpp) ; 7.58 (4 H, s, Dpp) ; 7.40 (8 H, d, Dpp) ; 5.10 (8 H, s, Cp) ; 4.59 (8 H, s, Cp).

MS (ESI): calculated for $C_{72}H_{44}Fe_2N_4O_8$ 1204.1 ; found 1205.3 $[M+1]^+$

Preparation of Dpp[Leu$_2$Boc]$_2$ (2)

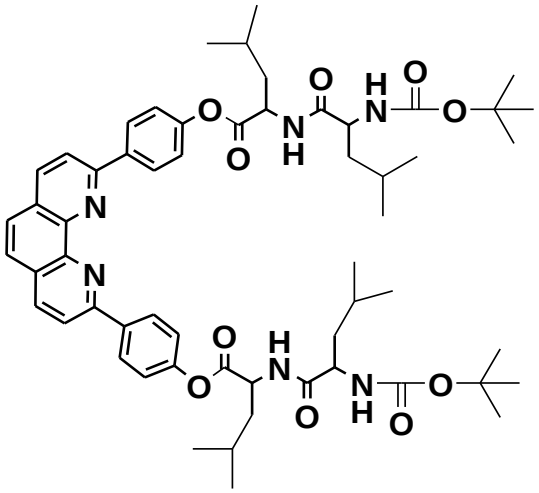

To a stirring solution of 183 mg (0.5 mmol) Dpp in 100 mL DCM, 378 mg (1.1 mmol) Boc-Leu$_2$-OH was added with TEA (0.25 mL) and allowed to cool on ice. 134 mg (1.1 mmol) DMAP and 340 mg (1.5 mmol) DCC were added sequentially and the reaction was removed from the ice and allowed to stir for 24h. The urea was filtered off, the solution subjected to aqueous workup described above and the organic phase evaporated to dryness. This is followed by column chromatography on SiO_2 (10%EtOAc:DCM. (1:9) (R_f = 0.60) (200 mg, 40%).

^{1}H NMR ($CDCl_3$, δ in ppm): 8.45 (4 H, d, Dpp), 8.30 (2 H, d, Dpp), 8.27 (1 H, d, NH), 8.09 (2 H, d, Dpp), 7.77 (2 H, s, Dpp), 7.31 (4 H, d, Dpp), 7.71 (1 H, s, NH), 7.03 (1 H, d, NH), 6.57 (1 H, d, NH), 4.99-4.85 (2 H, m, αCH), 4.63-4.44 (2 H, m, αCH), 4.19-3.99 (4 H, m, αCH),, 1.43 (18 H, s, Boc), 0.97-0.85 (24 H, d, Leu-CH_3). MS (ESI): calculated for $C_{58}H_{76}N_6O_{10}$ 1016.5 ; found 1017.3 $[M+1]^+$

Preparation of Fc[Leu$_2$]$_2$Dpp (3)

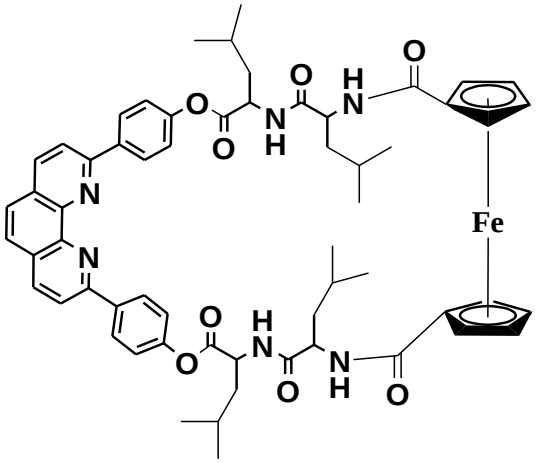

Compound **2** 180 mg (0.177 mmol) was dissolved in 2 mL DCM and 2 mL TFA was added. After 30 minutes, the mixture was dried in vacuo. Excess TFA was removed by repeated drying in vacuum and addition of DCM. The resulting solid was then dissolved in 600 mL in DCM and TEA and 100 mg K_2CO_3 were added to ensure the solution was at basic conditions. The resulting clear solution was then cooled and allowed to stir for 10 minutes. Ferrocene diacid chloride 55 mg (0.177 mmol) was then added drop wise over 24hrs and allowed to stir an additional 24h. The volume of the solution was then reduced to 100 mL and was washed with saturated $NaHCO_3$, 10% citric acid, and finally distilled H_2O. The organic phase was collected, dried over anhydrous Na_2SO_4, filtered, and then dried in vacuo. The compound was then purified by preparatory plate chromatography with a mobile phase of 4:1 EtOAc:Hex. (R_f = 0.63). The final product is believed to be reasonably clean with only minor impurities of side products from the reaction determined by NMR. Yield = 15 mg, 9%)

^{1}H NMR ($CDCl_3$, δ in ppm): 8.47 (4 H, d, Dpp), 8.44 (1 H, d, NH), 8.24 (2 H, d, Dpp), 8.01 (4 H, m, Dpp), 7.72 (2 H,s, Dpp), 7.32 (1 H, d, NH), 7.24 (1 H, d, NH), 7.15 (2 H, d, Dpp), 6.60 (1 H, d, NH), 4.81 (2 H, s, Cp), 4.69 (2 H, s, Cp), 4.59 (2 H, d, αCH), 4.45 (2

H, s, Cp), 4.28 (2 H, s, Cp), 3.98 (2 H, d, αCH), 1.95-1.77 (12 H, m, Leu-CH-CH_2), 1.05-0.85 (24 H, m, Leu-CH_3). MS (ESI): calculated for $C_{60}H_{66}FeN_6O_8$ 1254.4; found 1255.8 $[M+1]^+$

Preparation of Dpp[$Leu_3Boc]_2$ (4)

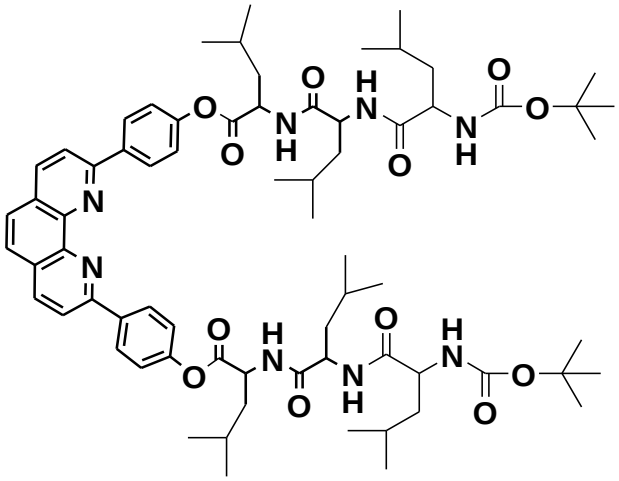

To a stirring solution of Dpp 934 mg (2.6 mmol) in 100 mL DCM, Boc-Leu_3-OH 2.8 g (0.1 mmol) was added with TEA 0.94 mL and allowed to cool on ice. DMAP (748 mg, 6.0 mmol) and DCC 1.5 g (6.1 mmol) were added sequentially as solids and the reaction was removed from the ice and allowed to stir for 24h. The resulting solution was dried in vacuo and filtered to remove urea side products. The solution was then washed with saturated $NaHCO_3$, 10% citric acid, and finally distilled H_2O and the organic phase was collected, dried over anhydrous Na_2SO_4, filtered and evaporated to dryness. Purification of the product was done by column chromatography (20%EtOAc:DCM).(R_f = 0.70). Yield = 1.8 g, 56 %.

^{1}H NMR ($CDCl_3$, δ in ppm): 8.45 (4 H, d, Dpp), 8.31 (2 H, d, Dpp), 8.11 (2 H, d, Dpp), 7.78 (2 H, s, Dpp), 7.29 (2 H, s, NH), 7.32 (4 H, d, Dpp), 7.07 (1 H, d, NH), 6.70 (1 H, d, NH), 6.53 (1 H, d, NH), 6.07 (1 H, d, NH), 4.87 (2 H, m, αCH), 4.67 (1 H, m, αCH), 4.52 (1 H, m, αCH), 4.08 (2 H, m, αCH), 1.85-1.68 (18 H, m, Leu-CH-CH_2), 1.47 (18 H, s, Boc), 1.01-0.87 (36 H, m, Leu-CH_3). MS (ESI): calculated for $C_{70}H_{98}N_8O_{12}$ 1242.7; found 1253.5 $[M+1]^+$

Preparation of Fc[Leu$_3$]$_2$Dpp (5)

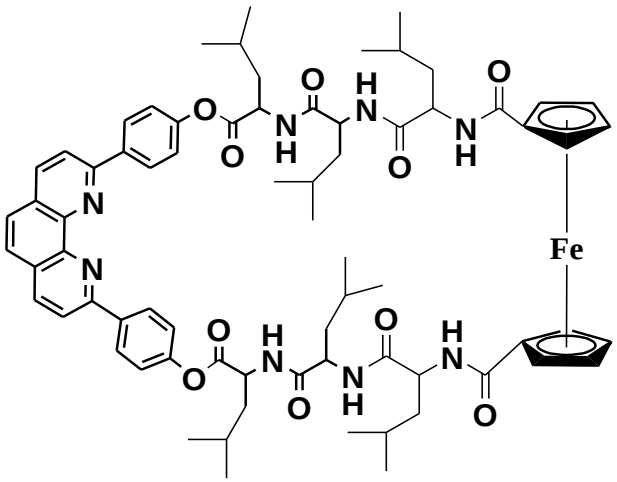

The procedure is identical to that described for the preparation of compound **2**. Compound **4** 400 mg (0.31 mmol) was dissolved in 2 mL DCM and 2mL TFA was added. Ferrocene diacid chloride 97 mg (0.31mmol) was added over 24h. Preparatory plate chromatography (SiO_2) with a mobile phase of 4:1 EtOAc:Hex. (R_f = 0.68) gave a yield of 30 mg (8%). The final product is believed to be reasonably clean with only minor impurities of side products from the reaction determined by NMR

^{1}H NMR ($CDCl_3$, δ in ppm): 8.41 (4 H, d, Dpp), 8.32 (1 H, d, NH), 8.26 (2 H, d, Dpp), 8.06 (2 H, d, Dpp), 7.98 (1 H, d, NH), 7.75 (2 H, s, Dpp), 7.25 (4 H, d, Dpp), 7.06 (1 H,

d, NH), 6.80 (2 H, d, NH), 6.34 (1 H, d, NH), 4.90-4.80 (2 H, m, αCH), 4.79-4.71 (3 H, m, αCH, Cp), 4.69-4.59 (3 H, m, αCH, Cp), 4.49-4.42 (1 H, m, αCH), 4.38-4.20 (2 H, m, Cp), 4.29-4.22 (3 H, m, αCH, Cp), 1.90-1.72 (18 H, m, Leu-CH-CH_2), 1.00-0.95 (36 H, m, Leu-CH_3). MS (ESI): calculated for $C_{72}H_{88}FeN_8O_{10}$ 1280.6; found 1281.5 $[M+1]^+$

Preparation of Dpp[GlyBoc]$_2$ (6)

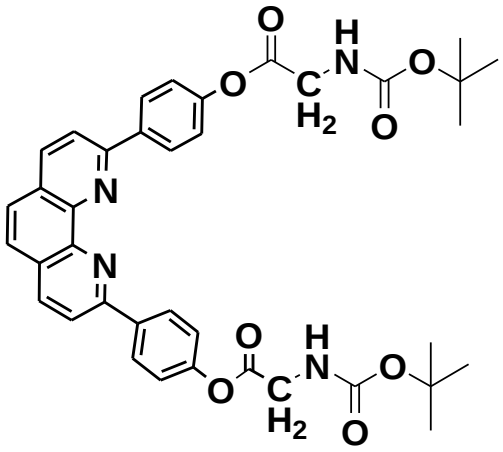

To a stirring solution of Dpp 183 mg (0.5 mmol) in 100 mL DCM, Boc-Gly-OH 192 mg (1.1 mmol) was added with TEA 0.25 mL and allowed to cool on ice. DMAP 134 mg (1.1 mmol) and DCC 340 mg (1.5 mmol) were added sequentially and the reaction was removed from the ice and allowed to stir for 24h. The resulting solution was dried by vacuum and filtered to remove urea side products. The reaction mixture was then subjected to a standard aqueous work described above. The organic phase was collected, dried over anhydrous Na_2SO_4, filtered, and evaporated to dryness. After column chromatography (SiO_2, 10%EtOAc:DCM.(R_f = 0.60), 203 mg of the desired product was obtained (Yield = 60%)

^{1}H NMR ($CDCl_3$, δ in ppm): 8.45 (4 H, d, Dpp), 8.30 (2 H, d, Dpp), 8.09 (2 H, d, Dpp), 7.77 (2 H, s, Dpp), 7.31 (4 H, d, Dpp), 5.08 (2 H, m, NH), 4.24 (αCH_2), 1.43 (18 H, s, Boc). MS (ESI): calculated for $C_{38}H_{38}N_4O_8$ 678.2; found 679.4 $[M+1]^+$

Preparation of Dpp[Leu-AlaBoc]$_2$ (7)

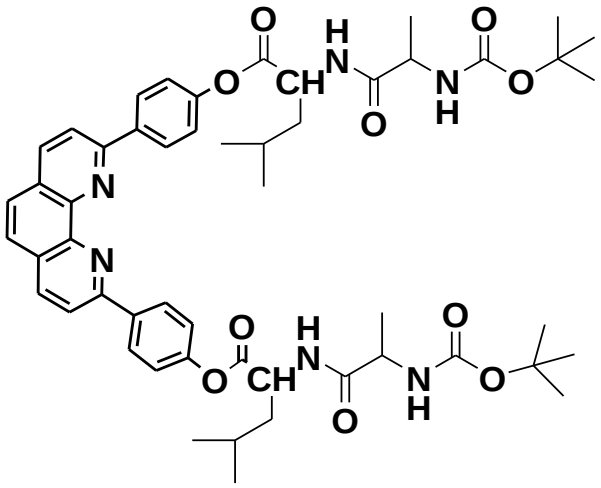

The synthetic procedure is identical to that described for compounds **2**, **4**, and **6**. Amounts used: Dpp 183 mg (0.5 mmol) in 100 mL DCM, Boc-Leu-Ala-OH 332 mg (1.1 mmol) DMAP 134 mg (1.1mmol), DCC 340 mg (1.5mmol) Column chromatography: SiO_2, 10%EtOAc:DCM.(R_f = 0.60). Yield: 265 mg, 55%

^{1}H NMR ($CDCl_3$, δ in ppm): 8.45 (4 H, d, Dpp), 8.30 (2 H, d, Dpp), 8.27 (2 H, d, Dpp), 7.85 (2 H, s, Dpp), 7.34 (4 H, d, Dpp), 6.65 (2H, d, NH), 5.02 (2H, d, NH), 4.99-4.85 (2 H, m, αCH), 4.25 (2 H, m, αCH), 1.60 (6 H, m, Leu-CH-CH_2), 1.49 (18 H, s, Boc), 1.40 (6H, d, Ala-CH_3), 1.03 (12H, m, Leu-CH_3). MS (ESI): calculated for $C_{52}H_{64}N_6O_{10}$ 932.4; found 933.7 $[M+1]^+$

Preparation of [Fc(n'-Ala-OMe)(1-Gly)]$_2$-1,4-butyl diamine (8) :

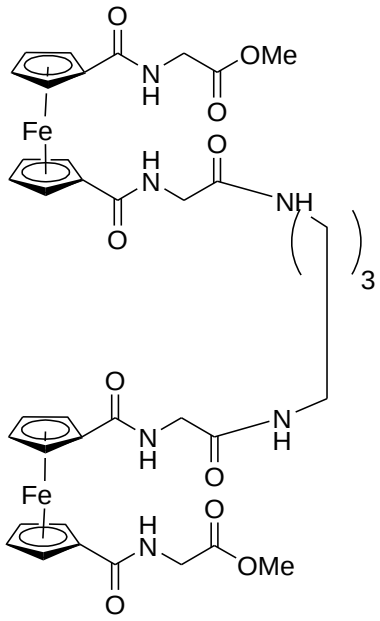

Fc(n`-Gly-OMe)(1-Gly-OH) was prepared by partial hydrolysis of Fc(1-n`-Gly-OMe)$_2$. Fc(n`-Gly-OMe)(1-Gly-OH) 40mg (0.1 mmol) is stirred in 50 mL DCM with 1.5 eq EDC 24 mg (0.15 mmol) and HOBt (21 mg, 0.15 mmol) for 30 min. After the activation of the acid to a activated ester is completed the solution is diluted to 200 mL DCM and a solution of 0.5 eq of 1,4-butyl diamine 4 mg (0.05 mmol) is added dropwise. The solution is then stirred overnight, evaporated to dryness and subjected to an aqueous workup as described above. The organic phase was collected, dried over anhydrous Na_2SO_4, filtered, and evaporated to dryness. The compound was then purified by column chromatography with a mobile phase of 95:5 $CHCl_3$:MeOH. (R_F = 0.32). Yield = 12% (0.009 g)

^{1}H NMR ($CDCl_3$, δ in ppm): 9.33 (2 H, d, Gly-NH), 8.43 (2 H, d, Linker-NH), 8.34 (2 H, d, Gly-NH), 4.90(4 H, s, Cp), 4.84 (4 H, s, Cp), 4.47 (4H, s, Cp), 4.39 (4H, s, Cp), 4.14 (4 H, d, αCH_2), 3.93 (4 H, d, αCH_2), 3.83 (6 H, s, OMe), 3.41 (4H, s, Linker-CH_2), 1.72 (4H, s, Linker-CH_2). MS (ESI): calculated for $C_{38}H_{45}Fe_2N_6O_{10}$ 857.2 ; found 858.2 $[M+1]^+$

Preparation of [Fc(n'-Ala-OMe)(1-Ala)]$_2$-1,4-butyl diamine (9) :

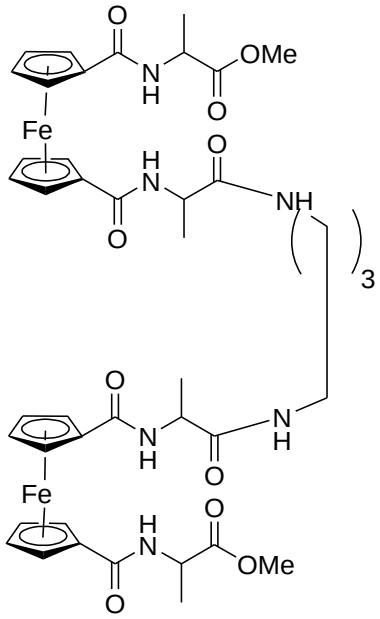

The procedure is identical to that described for compound **8**. Fc(n`-Ala-OMe)(1-Ala-OH) was prepared by partial hydrolysis of Fc(1-n`-Ala-OMe)$_2$. Amounts: Fc(n`-Ala-OMe)(1-Ala-OH) 25 mg (0.05 mmol), 50 mL DCM with 1.5eq EDC 10 mg (0.075 mmol) and HOBt 10 mg (0.075 mmol) Dilution to 200 mL DCM, 0.5eq 2 mg (0.025 mmol) of 1,4-

butyl diamine. Purification by column chromatography 95:5 $CHCl_3$:MeOH (R_F = 0.32). Yield = 20% (0.011g).

^{1}H NMR ($CDCl_3$, δ in ppm): 8.97 (2 H, d, Ala-NH), 8.56 (2 H, d, Linker-NH), 7.95 (2 H, d, Ala-NH), 4.93(6 H, s, Cp), 4.91 (2 H, m, αCH), 4.89 (2H, d, Cp), 4.78 (2H, m, αCH), 4.58 (2 H, s, Cp), 4.34 (4 H, s, Cp), 4.32 (2 H, s, Cp), 3.84 (6 H, s, OMe), 2.95 (4H, d, Linker-CH_2), 1.86 (4H, m, Linker-CH_2), 1.56 (6 H, d, Ala-CH_3), 1.35 (6 H, d, Ala-CH_3).MS (ESI): calculated for $C_{42}H_{53}Fe_2N_6O_{10}$ 913.3; found 914.1 $[M+1]^+$.

REFERENCES

1. Merriam-Webster. (2001). Merriam-Webster's collegiate dictionary. (10^{th} Ed.). U.S.A. Merriam-Webster.
2. Avetisov VA, Goldanskii VI, Kuzmin VV. Phys. Today. 44, 33-41, **1991**.
3. Vvtugyi R, Mezo G, Fellinger E, Andreu D, Hudecz F. J. Pept. Sci. 11, 642-649, **2005.**
4. Luckett S, Garcia RS, Barker JJ, Konarev AV, Shewry PR, Clarke AR, Brady RL. J. Mol. Biol. 290 , 525-533, **1999**.
5. Eisenbrandt R, Kalkum M, Lai EM, Lurz R, Kado CI, Lanka E. J. Biol. Chem. 274 , 22548-22555, **1999**.
6. Maqueda M, Galvez A, Bueno MM, Sanchez-Barrena MJ, Gonzalez C, Albert A, Rico M, Valdivia E. Curr. Protein Pept. Sci. 5, 399-416, **2004**.
7. Craik DJ. Science. 311, 1563-1564, **2006**.
8. Galvez A, Gimenezgallego G, Maqueda M, Valdivia E. Antimicrob. Agents. Ch. 33, 437-441, **1998**.
9. Cole AM, Hong T, Boo LM, Nguyen T, Zhao CQ, Bristol G, Zack JA, Waring AJ, Yang OO, Lehrer RI. Proc. Natl. Acad. Sci. U.S.A. 99, 1813-1818, **2002**.
10. Bulet P, Stocklin R, Menin L. ImmunoI. Rev. 198, 169-184, **2004.**
11. Hallock YF, Sowder RC, Pannell LK, Hughes CB, Johnson DG, Gulakowski R, Cardellina JH, Boyd MR. J. Org. Chem. 65, 124-128, **2000**.
12. Craik DJ, Daly NL, Waine C. Toxicon. 39, 43-60, **2001**.
13. Tran D, Tran P, Roberts K, Osapay G, Schaal J, Ouellette A, Selsted ME. Antimicrob. Agents. Ch. 52, 944-953, **2008**.
14. Rosengren KJ, Daly NL, Plan MR, Waine C, Craik DJ. J. Biol. Chem. 278, 8606-8616, **2003**.
15. Grande MJ, Lucas R, Abriouel H, Valdivia E, Ben Omar N, Maqueda M, Martinez-Bueno M, Martinez-Canamero M, Galvez A. Int. J. Food Microbiol. 106, 185-194, **2006**.
16. Clark RJ, Daly NL, Craik DJ. Biochem. J. 394, 85-93, **2006**.
17. Zhang LS, Tam JP. Tetrahedron Lett. 38, 4375-4378, **1997**.
18. Cousins GRL, Poulsen SA, Sanders JKM. Curr. Opin. Chem. Biol. 4, 270-279, **2000**.
19. Brady SF, Varga SL, Freidinger RM, Schwenk DA, Mendlowski M, Holly FW, Veber DF. J. Org. Chem. 44, 3101-3105, **1979**.
20. Kates SA, Sole NA, Johnson CR, Hudson D, Barany G, Albericio F. Tetrahedron Lett. 34, 1549-1552, **1993**.
21. Jensen KJ, Alsina J, Songster MF, Vagner J, Albericio F, Barany G. J. Am. Chem. Soc. 120, 5441-5452, **1998**.
22. Ranganathan D, Haridas V, Karle IL. J. Am. Chem. Soc. 120, 2695-2702, **1998**.
23. Huang H, Mu LJ, He JQ, Cheng JP. J. Org. Chem. 68, 7605-7611**, 2003**.
24. Fustero S, Sanchez-Rosello M, Rodrigo V, Sanz-Cervera JF, Piera J, Simon-Fuentes A, del Pozo C. Chem-Eur. J. 14, 7019-7029, **2008**.
25. Orlowski GA, Chowdhury S, Kraatz HB. Electrochim. Acta. 53, 2034-2039, **2007**.
26. Orlowski GA, Chowdhury S, Kraatz HB. Langmuir. 23. 12765-12770, **2007**.

27. Moriuchi T, Nagai T, Hirao T. Org. Lett. 8, 31-34, **2006**.
28. Chowdhury S, Sanders DAR, Schatte G, Kraatz HB. Angew. Chem. Int. Edit. 45, 751-754, **2006.**
29. Dietrich-Buchecker C, Sauvage J.P. Tetrahedron. 46, 503-512, **1990**.
30. Gloe, K. (2005) Macrocyclic Chemistry: Current Trends and Future Perspectives. Netherlands: Springer
31. Blackwell HEE, Grubbs RHH. Angew. Chem. Int. Edit. 37, 3281-3284, **1998**.
32. Jackson S, Degrado W, Dwivedi A, Parthasarathy A, Higley A, Krywko J, Rockwell A, Markwalder J, Wells G, Wexler R, Mousa S, Harlow R. J. Am. Chem. Soc. 116, 3220-3230, **1994**.
33. Moriuchi T, Yoshida K, Hirao T. Organometallics. 20, 3101-3105, **2001**.
34. Neises B, Steglich W Angew. Chem. Int. Edit. 17, 522-524, **1978**.
35. Hubbard P, Brittain WJ. J. Org. Chem. 63, 677-683, **1998**.
36. Meah MNN, Sanders JKM. J. Am. Chem. Soc. 112, 5773-5780, **1990**.
37. Nishio M, Hirota M, Umezawa Y. (1998). The Ch/Π Interaction. New-York: Wiley-Vch.
38. Lin L, Berces A, Kraatz HB. J. Organomet. Chem. 556, 11-20, **2004**.
39. Lindner E, Zong RF, Strobele M, Eichele K. Z. ANORG. ALLG. CHEM. 629, 587-588, **2003**.
40. Kirin SI, Schatzschneider U, de Hatten X, Weyhermuller T, Metzler-Nolte N. J. Organomet. Chem. 691, 3451-3457, **2006**.
41. Wu YW, Wang RJ, Jiang YY, Fu H, Zhao YF. Acta. Crystallogr. C. 60, O178-O179, **2004**
42. Ding Y, Mei Y, Zhang JZH, Tao FM. J. Comput. Chem. 29, 275-279. **2008**.
43. Sheu SY, Selzle HL, Schlag EW, Yang DY. Chem. Phys. Lett. 462, 1-5, **2008**.
44. Cesario M, Dietrichbuchecker CO, Guilhem J, Pascard C, Sauvage JP. J. Chem. Soc. Chem. Comm. 5, 244-247, **1985**.
45. Champin B, Sartor V, Sauvage JP. New. J. Chem. 32, 1048-1054, **1008**.
46. Beer PD, Gale PA, Chen GZ. Coordin. Chem. Rev. 185, 3-36, **1999**.
47. Plenio H, Burth D. Organometallics. 15, 4054-4062, **1996.**
48. Beer PD, Danks JP, Hesek D, Mcaleer JF. J. Chem. Soc. Chem. Comm. 23, 1735-1737, **1993**.
49. Tsierkezos NG. J. Solution. Chem. 36, 289-302, **2007**.
50. Cui XL, Carapuca HM, Delgado R, Drew MGB, Felix V. Dalton Trans. 11, 1743-1751, **2004**.
51. Beer PD, Chen Z, Drew MGB, Johnson AOM, Smith DK, Spencer P. Inorg. Chim. Acta. 246, 143-150, **1996**.
52. Appoh FE, Sutherland TC, Kraatz HB. J. Organomet. Chem. 690, 1209-1217, **2005**.
53. Guo DS, Liu ZP, Ma JP, Huang RQ. Tetrahedron. Lett. 48, 1221-1224, **2007**.
54. Poon KW, Yan Y, Li XY, Ng DKP. Organometallics. 18, 3528-3533, **1999**.
55. Sabel DM, Thompson JA, Butcher R, Smith PH. Acta. Crystallogr. C. 52, 1950-1954, **1996**.
56. Herrick RS, Jarret RM, Curran TP, Dragoli DR, Flaherty MB, Lindyberg SE, Slate RA Thornton LC. Tetrahedron Lett. 37, 5289, **1996**.

57. a) Chantson JT, Falzacappa MVV, Crovella S, Metzler-Nolte N, J. Organomet. Chem. 690, 4564, **2005**. b) Noor F, Wüstholz A, Kinscherf R, Metzler-Nolte N. Angew. Chem. Int. Ed. 44, 2429, **2005**. c) Goel A, Savage D, Alley SR, Kelly PN, O'Sullivan D, Mueller-Bunz H, Kenny PTM. J. Organometal. Chem. 692, 1292, **2007**.
58. a) Bediako-Amoa I, Silerova R, Kraatz HB. Chem. Commun. 2430, **2002**. b) Bediako-Amoa I, Sutherland TC, Li CZ, Silerova R, Kraatz HB. J. Phys. Chem. B 108, 704, **2004**.
59. a) Kraatz HB, Lusztyk J, Enright GD, Inorg. Chem. 36, 2400, **1997**.b) Mahmoud KA, Long YT, Schatte G, Eur. J. Inorg. Chem. 173, **2005**.
60. Chowdhury S, Schatte G,Kraatz HB. Angew. Chem. Int. Edit. 45, 6882-6884, **2006**.
61. Chowdhury S, Mahmoud KA, Schatte G, Kraatz HB. Org. Biomol. Chem. 3, 3018-3023, **2005**.
62. Beer PD, Cadman J, Lloris JM, Martinez-Manez R, Padilla ME, Pardo T, Smith DK. J.Dalton Trans. 2, 127-133, **1999**.
63. Debroy P, Roy S. Coord. Chem. Rev. 251, 203-221, **2007.**
64. Merriam-Webster. (2001). Merriam-Webster's collegiate dictionary. (10^{th} Ed.). U.S.A. Merriam-Webster.
65. Wikoff WR, Liljas L, Duda RL, Tsuruta H, Hendrix RW, Johnson JE. Science, 289, 2129-2133, **2000**.
66. Blankenship JW, Dawson PE. J. Mol. Biol. 327, 537-548, **2003.**
67. Boutz DR, Cascio D, Whitelegge J, Perry LJ, Yeates TO. J. Mol. Biol. 368, 1332-1344, **2007**.
68. Blankenship JW, Dawson PE. Protein Sci. 16, 1249-1256, **2007**.
69. Zhou HX. J. Am. Chem. Soc. 125, 9280-9281, **2003**.
70. Wang XY, Bao XF, McFarland-Mancini M, Isaacsohn I, Drew AF, Smithrud DB. J. Am. Chem. Soc. 129, 7284-7293, **2007**.
71. Green JE, Choi JW, Boukai A, Bunimovich Y, Johnston-Halperin E, DeIonno E, Luo Y, Sheriff BA, Xu K, Shin YS, Tseng HR, Stoddart JF, Heath JR. Nature. 445, 414-417, **2007**.
72. Chatterjee MN, Kay ER, Leigh DA. J. Am. Chem. Soc. 128, 4058-4073, **2006.**
73. Jager R, Vogtle F. Angew. Chem. Int. Ed. 36, 930-944, **1997**
74. Talley JM, Cerda BA, Ohanessian G, Wesdemiotis C. Chem. Eur. J. 8, 1377-1388, **2002**.
75. Tan XS, Fujii Y, Sato T, Nakano Y, Yashiro M. Chem. Comm. 10, 881-882, **1999**.
76. Diaddario LL, Robinson Wr, Margerum Dw. Inorg. Chem. 22, 1021-1025, **1983**.
77. Rapic V, Schlogl K, Steinitz B. J. Organomet. Chem. 94, 87-98, **1975**
78. Khan MSU, Nigar A, Bashir MA, Akhter Z. Synth. Commun. 37, 473-482, **2007**.
79. Dietrich-Buchecker CO, Marnot PA, Sauvage JP. Tetrahedron Lett. 23, 5291-5294, **1982**.